A Program of Spin-Dependent Electron Scattering from a Polarized ^{3}He Target in CLAS12

R. Cruz-Torres, A. Denniston, I. Friščić, D. Hasell, F. Hauenstein, O. Hen, R. Johnston, J. Kahlbow, T. Kutz, S. Lee, P. Moran, R. Milner, D. Nguyen, J. Pybus, E. Segarra, H. Szumila-Vance, Y. Wang

Laboratory for Nuclear Science, MIT, Cambridge, MA

H. Avakian, M. Battaglieri, J. Brock, V. Burkert, L. Elouadrhiri, D.W. Higinbotham, V. Kubarovsky, C. Keith, J. Maxwell, D. Meekins, V. Mokeev, R. Paremuzyan, A. Prokudin, P. Rossi, C. Weiss

Thomas Jefferson National Accelerator Facility, Newport News, VA

V. Bellini, C. Petta, C. Sutera, F. Tortorici

INFN Catania and University of Catania, Italy

S. Bastami, R. Capobianco, S. Diehl, F.-X. Girod, K. Joo, A. Kim, V. Klimenko, R. Santos, P. Schweitzer, P. Stoler, K. Tezgin

University of Connecticut, Storrs, CT

C. Dilks, A. Vossen

Duke University Durham, NC

F. Benmokhtar, A. Boyer, A. Gadsby, A. Parker

Duquesne University, Pittsburgh, PA

L. Barion, G. Ciullo, M. Contalbrigo, P. Lenisa, L. Pappalardo, A. Movsisyan

University of Ferrara, Italy

M. Mirazita, P. Rossi, O.Soto

INFN-LNF, Frascati, Italy

A. Celentano, R. De Vita, M. Ripani, M. Osipenko

INFN-Genova, Italy

A. Schmidt

George Washington University, Washington, DC

B. McKinnon, D. Sokhan

University of Glasgow, United Kingdom

M. Mihovilovič, S. Širca

University of Ljubljana, Slovenia

P. Stoler

Rennsalaer Polytechnic Institute, Troy, NY

A.M. Kotzinian, B. Parsamyan

INFN-Torino, Turin, Italy

P. Kroll

University of Wuppertal, Germany

and the CLAS12 collaboration.

Co-Spokespeople: Harut Avakian, James Maxwell, Richard Milner[a], Dien Nguyen

(Dated: June 21, 2020)

[a]milner@mit.edu

Abstract

We propose a program of spin-dependent electron scattering using a polarized electron beam of intensity 2.5 μA at an energy of 10.6 GeV incident on a novel polarized ^{3}He gas target taking data at a luminosity of 4.5×10^{34} ^{3}He/cm^2/s located within the central solenoid of the CLAS12 spectrometer in Hall B. In this initial proposal, we request 30 PAC days of beamtime to carry out precision measurements of spin-dependent inclusive and semi-inclusive DIS ($\pi^{\pm}$ and K$^{\pm}$) directly from a longitudinally polarized neutron over a large kinematic range: $0.05 < x < 0.7$, $1 < Q^2 < 9$ (GeV/c)^2, $0.2 < z < 0.9$, $0 < P_T < 1.3$ GeV/c with the purpose of extracting the flavor dependence of the quark polarizations and, in particular, determining their transverse momentum dependence. High precision 5-D (x, z, P_T, Q^2, ϕ_h) data on the neutron, in a kinematic region inaccessible and complementary to EIC, will constrain present theoretical ideas of the spin structure of the nucleon described by QCD. The nuclear corrections for SIDIS for the polarized neutron in ^{3}He will be different from those on the deuteron and a combined data set from CLAS12 on both targets will offer an unprecedented opportunity to study the spin-dependent in-medium hadronization process. The proposed experiment is competitive with both the approved CLAS Run Group C experiments on the deuteron and a possible future experiment using the proposed SoLID detector.

I. EXECUTIVE SUMMARY

We request 30 PAC days to exploit a recent technical advance in the polarization of ^{3}He. High-field MEOP, developed by a BNL-MIT collaboration for a polarized ^{3}He ion source at RHIC/EIC, when applied to a cryogenically cooled double-cell polarized ^{3}He target system developed at Caltech and used successfully at MIT-Bates, allows the possibility to locate a polarized ^{3}He gas target in the central 5 T solenoid of the CLAS12 spectrometer with a luminosity equal to the maximum design value.

With the 10.6 GeV highly polarized CEBAF beam, such a target and the CLAS12 spectrometer can enable the measurement of the spin-dependent asymmetry across the complete inelastic spectrum for both longitudinally and transversely polarized target. In this initial proposal, we focus on measurement of spin-dependent DIS, SIDIS ($\pi^\pm$ and K$^\pm$) and di-hadrons ($\pi^+\pi^-$) from a longitudinally polarized target. It is proposed to carry out precision measurements of the inclusive spin-dependent structure functions of the neutron over the kinematic range $0.05 < x < 0.7$ and $1 < Q^2 < 9$ (GeV/c)^2 and to precisely measure SIDIS and di-hadron reactions over $0.2 < z < 0.9$ and $0 < P_T < 1.3$ (GeV/c).

The proposed experiment will provide a data set that is complementary to the planned measurements on an ND_3 target in CLAS12. The principal scientific aims of this proposal are:

- to study the nuclear corrections to SIDIS in polarized ^{3}He, compare them to those for the deuteron and confront the current theoretical understanding of the hadronization process in light nuclei,
- to extract the P_T dependence of the longitudinal spin structure and constrain the current theoretical understanding.

The combined spin-dependent DIS and SIDIS precision data on the deuteron and ^{3}He targets from CLAS12 will open a new window into the hadronization process in light nuclei. Further, there is a natural evolution to further experiments, where the target is transversely polarized and detection of recoil particles and exclusive final-states is implemented.

II. INTRODUCTION

The upgraded 11 GeV CEBAF polarized electron beam offers the unprecedented opportunity to understand the valence quark structure of matter over the next decade and beyond. In particular, the operating CLAS12 spectrometer in Hall B with its ability to measure the multi-particle final-state in electron scattering from the nucleon and nuclei at high collision luminosities $\sim 10^{35}$ nucleons/cm^2/s over the complete kinematic range is the basis for the approved world-class program on the proton, polarized proton and deuteron and nuclei. Polarized targets (both longitudinal and transverse to the incident beam direction) offer the ability to utilize spin in the most effective way to access new observables like GPDs and TMDs that are at the frontiers of understanding the fundamental structure of matter and directly lead to the future Electron-Ion Collider (EIC).

The ^{3}He nucleus has long occupied a special place in nuclear physics. The significantly bound three-nucleon system, in comparison to the deuteron, has a rich spin-isospin momentum structure, and has been the focus of sophisticated theoretical studies over decades [1]. Polarized ^{3}He gas targets using optical pumping have been successfully developed [2] and used in electron scattering experiment since the late 1980s. It is accepted that in high-energy electron scattering a polarized ^{3}He nucleus is a very effective polarized neutron target. Thus, we believe that a polarized ^{3}He target internal to the existing CLAS12 spectrometer would enable a powerful, new program that takes advantage both of the upgraded CEBAF beam and the CLAS12 spectrometer and complements the existing, approved program on the polarized proton [3] and deuteron [4]. Our proposal offers direct access to the neutron using a completely independent target technology. In addition, it is complementary to the approved experiments with polarized ^{3}He targets in Hall A [5–7] as CLAS12 covers a significantly larger kinematic range compared to a conventional spectrometer.

Here, we request beam time to initiate a program of spin-dependent electron scattering from a polarized ^{3}He target internal to the CLAS12 detector and located within the central solenoid. The target concept [8], described in section III is based on existing technology and, if resources are available, could be realized quickly.

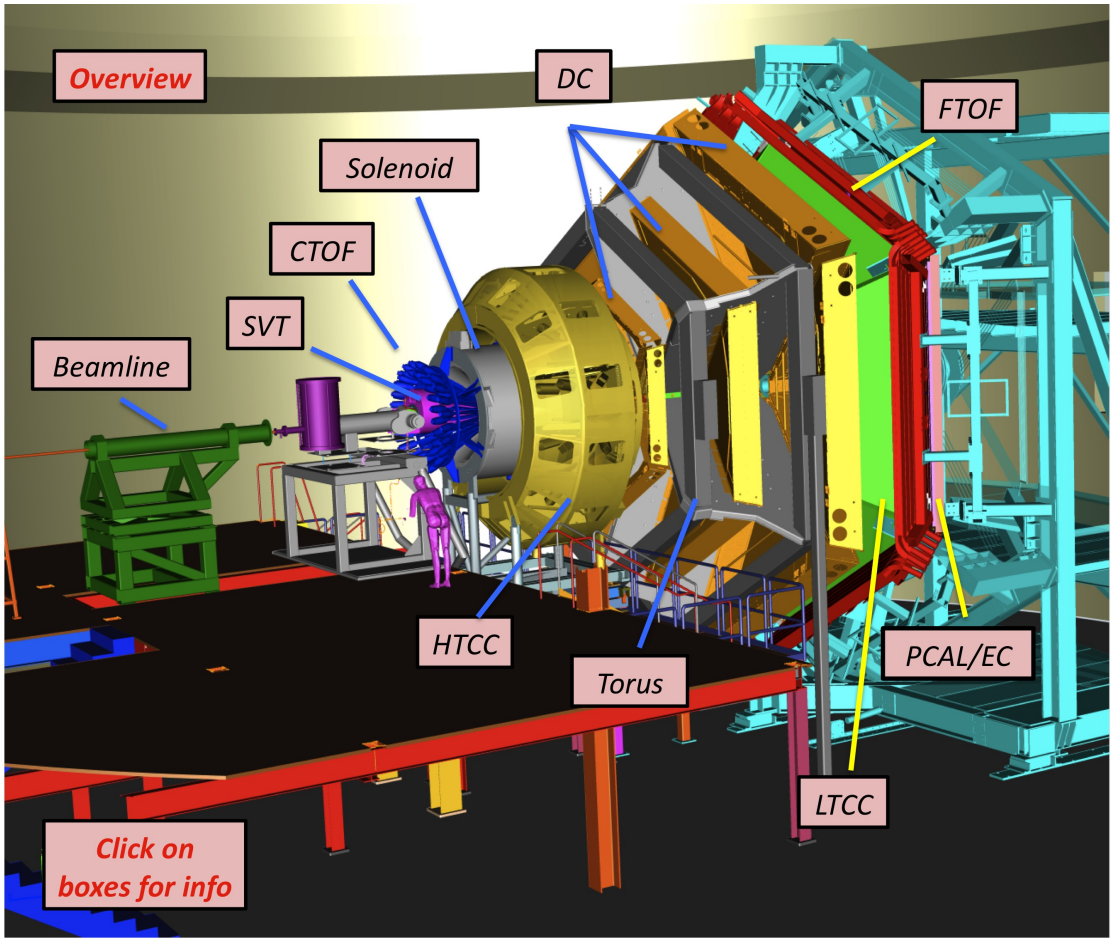

FIG. 1: Overview of the CLAS12 Spectrometer.

III. POLARIZED ^{3}HE TARGET

Due to the high magnetic field in the target region, traditional polarized ^{3}He targets are not available for use in CLAS12 without significant changes to the configuration and abilities of the spectrometer. A novel, high-field polarized ^{3}He target, compatible with Hall B's standard configuration, will take advantage of recent improvements in high-field metastability exchange optical pumping (MEOP) to create 60% polarized ^{3}He gas and reach CLAS12's luminosity limit with a 2.5 μA beam current. The gas will be polarized within the 5 T solenoid in a glass pumping cell at room temperature and 100 mbar before being convectively transferred to an aluminum target cell held at 5 K through heat exchange with a liquid helium supply. A scheme to provide transverse polarization is being pursued, adapting the HD-Ice transverse proposal to cancel the longitudinal solenoidal field and establish a transverse holding field using bulk superconductor shielding.

A. High-Field Polarized ^{3}He

Jefferson Lab has a long and successful history undertaking spin-dependent scattering measurements of nuclear structure using polarized ^{3}He gas targets produced via spin exchange optical pumping (SEOP). These SEOP targets have made impressive leaps forward in achievable figure of merit since their first uses at SLAC, but due to increasing wall relaxation at high magnetic fields [9], they are not available for use in CLAS12. Another method for producing polarized ^{3}He gas, metastability exchange optical pumping (MEOP) [2], has historically had restrictive limits on the pressure at which it is effective, making it a less attractive method for high luminosity scattering experiments. However, before the advent of modern SEOP targets, the MIT-Bates 88-02 target used polarized ^{3}He gas via MEOP at room temperature and 2.6 mbar, increasing the target density by transferring this gas to a second target cell held at 17 K [10]. Recent developments in MEOP polarization have extended the pressure and magnetic field range at which it can be efficiently performed, and combined with the MIT-Bates 88-02 double cell design, they offer a path forward for a polarized ^{3}He target in CLAS12.

In MEOP, an RF plasma excites a small population of ^{3}He atoms into the 2^3S_1 metastable state, which can be optically pumped using circularly polarized laser light. Through metastability exchange collisions, the metastable atoms polarize ground-state atoms, and coupling between the electronic and nuclear spins transfers that polarization to the ^{3}He nuclei. With increasing magnetic field, Zeeman splitting acts to decouple the electronic and nuclear spins, reducing the efficiency of MEOP and leading to a conventional wisdom that effective high-field MEOP was impossible above 0.1 T. However, research at the Laboratoire Kastler Brossel at ENS in Paris, France—motivated by polarization for medical imaging in the presence of MRI magnets above 1 T—showed that MEOP is not only possible at high magnetic fields, but these high fields allow high steady-state polarization at higher pressures [11]. In 2004 they achieved 90% steady state polarization at 1.5 T and 1 mbar, and by 2013 they had reached greater than 50% polarization at 4.7 T and 100 mbar [12]. While increasing the magnetic field does act to decouple the electron and nuclear spins, slowing transfer of polarization to the nucleus, this decoupling also inhibits polarization relaxation channels. In addition, the separation of hyperfine states creates highly absorbing lines, where clearer discrimination of polarizing transitions is possible with the pumping laser while avoiding

depolarizing transitions. These high-field MEOP techniques are already being applied for nuclear physics applications as the basis of a polarized ^{3}He ion source for use at the Electron-Ion Collider, as pursued by the BNL Collider-Accelerator Department, R. Milner's group at MIT, and J. Maxwell of JLab [13].

B. Proposed Polarized ^{3}He Target for CLAS12

The proposed polarized ^{3}He target for CLAS12 will combine two proven techniques—high-field MEOP polarization and double-cell MEOP targets—to create a novel, high-luminosity, polarized ^{3}He target that operates in a high magnetic field environment. Figure 2 shows a diagram of the proposed design, with two gas cell volumes in convective contact—one cooled by a liquid helium heat exchanger, the other heated and optically pumped. Using 100 mbar gas in a 20 cm long aluminum target cell at 5 K will result in a target thickness of 3×10^{21} ^{3}He/cm^2, which at a beam current of 2.5 μA will produce 4.5×10^{34} ^{3}He/cm^2/s, reaching CLAS12's maximum per nucleon luminosity limit.

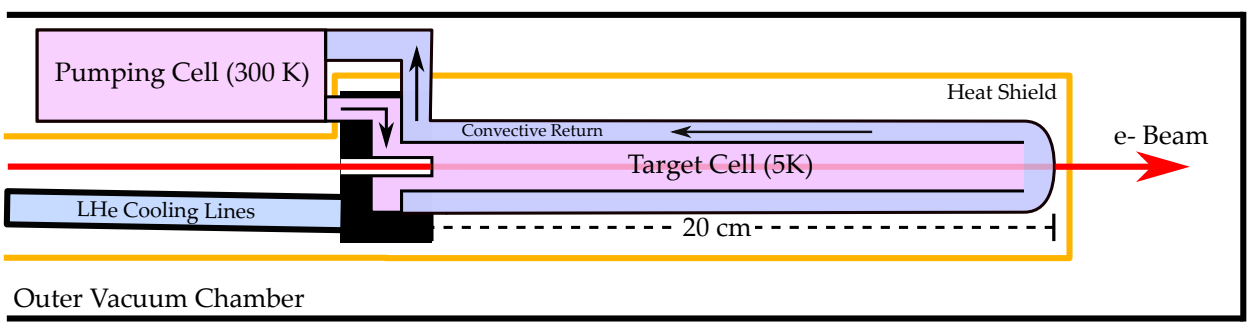

FIG. 2: Sideview layout of the polarized ^{3}He target.

Figure 3a shows the steady-state nuclear polarization versus gas pressure from ENS [2], illustrating the increase in achieved polarization with high magnetic field. These results indicate that 60% polarization should be possible at 100 mbar and 5 T without further improvements in the method. The polarization will be monitored using probe laser polarimetry, which uses the absorption ratios of two hyperfine states to observe the nuclear polarization [14]. Since only ratios of spectral amplitudes are involved, all experimental parameters affecting the absolute absorption intensities, such as fluctuations in laser power, are canceled out. Figure 3b shows example probe absorption peaks at 3 T and 1.3 mbar, with the gas at zero polarization (in blue circles) and near 90% (in red squares). By per-

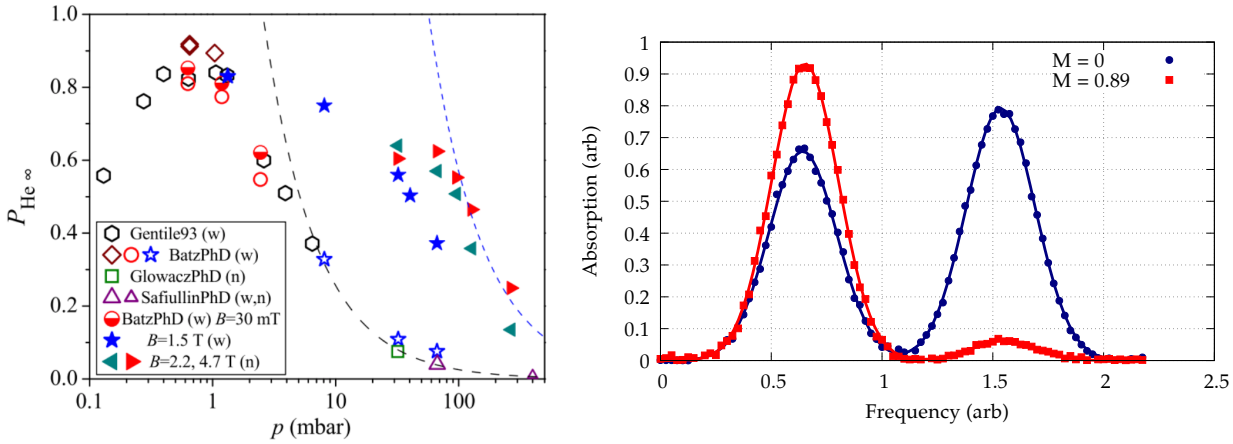

(a) Polarization versus pressure [2].

(b) Probe peaks at 3 T [15].

FIG. 3: World steady state MEOP polarization versus pressure at various magnetic fields (left), and probe peaks (right), shown as laser absorption versus frequency, for nuclear polarizations of 0 and 89% at 3 T and 1.3 mbar.

forming this measurement in the pumping cell, the polarization in the target can be inferred using the rate of gas transmission between the cells, as was done for the MIT-Bates 88-02 target [10]. Pulse NMR methods are also being investigated for localized polarization measurements. The polarization orientation can be flipped by reversing the circular polarization of the pumping light; pumping rates measured by the ENS group at 96 mbar were around 0.005 s^{-1} [12]. MEOP pumping rates are much faster than typical SEOP targets; taking into account the populations of our expected target and pumping cells, a switch should take less than 45 minutes. Should faster flipping times be required, adiabatic fast passage methods are frequently utilized with ^{3}He polarization systems [2].

The main sources of polarization relaxation come from wall interactions, transverse magnetic field gradients, and ionization in the beam. To avoid depolarization on the cell walls, the room temperature pumping cell will be made of borosilicate glass, and the aluminum target cell will be coated with a cryogenic layer of H_2, which has been shown to yield days long relaxation times between 2 and 6 K [16]. The transfer line itself will be glass transitioning to metal, where all metal parts will be cold enough to facilitate the cryogenic coating. The CLAS12 solenoid field map has been used to assess the rate of relaxation from transverse field gradients in the target region, as seen in Figure 4a, which showed that the field uniformity is more than sufficient [8]. Ionizing radiation can induce spin relaxation through the production of molecular $^3He_2^+$. This effect was studied extensively for the Bates 88-02

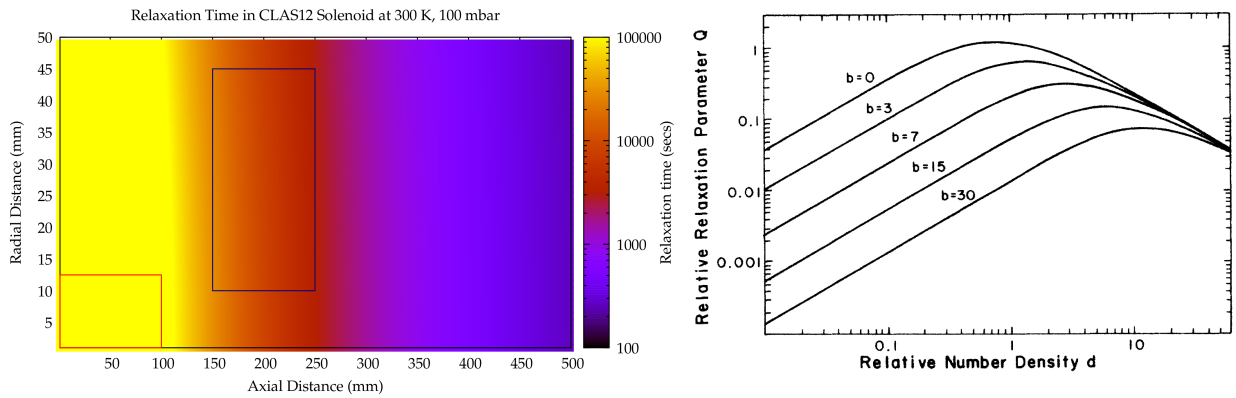

(a) Relaxation rate map [15].

(b) Relaxation rate vs. number density [18].

FIG. 4: Figure 4a shows the relaxation due to transverse magnetic field gradients in the space of the solenoid, showing candidate locations of the target cell in the center of the solenoid (in red), and the pumping cell upstream (in blue). Figure 4b shows the relative relaxation rate vs. number density, showing the decrease in the relaxation rate with increased magnetic field.

target [17], and was found to create a 2000 second relaxation time in 2.6 mbar gas under a beam current of 5μA. While the molecular production increases with density, increasing the magnetic field reduces the depolarization rate from to diatomic molecules. Figure 4b gives the relative relaxation rate vs. gas number density, showing the strong effect of increased magnetic field, here expressed as a relative value b, the ratio of the holding field over the atom's characteristic field. An increase in field from 10 G to 200 G, reduces the relaxation rate by two orders of magnitude as the rotational angular momentum spin is decoupled from the total molecular-ion spin [18]. The rate of communication between the cells, delivering polarization from the pumping cell to the target cell, will be studied extensively to ensure that the design promotes sufficient convection to maintain high polarization in the target cell.

A desire to reach the maximum luminosity of the detector has informed our choice of target length and beam current. The highest gas density we can achieve is limited by the temperature and pressure, which is in turn chosen based on the polarization we can sustain, for now based on data from ENS in Figure 3a. While the target length is constrained by the uniform field region of the magnet and the rate of transit of the gas through the cells, it may be possible to extend the target beyond our initial 20 cm design. The current power limit on the beam dump is 5 kW, which corresponds to 0.5 μA at 10 GeV, although Hall B is currently preparing a design for a beam dump upgrade to accommodate the ALERT

experiment, which would extend its power rating to 10 kW, or 1 μA at 10 GeV [19]. Our current target scheme would require this to be extended to 25 kW to reach 2.5 μA. Along with development of the target method, continued discussions with the Hall B staff involved in the beam dump upgrade will inform an optimization of the target length and beam current to maximize our physics impact in the allotted run schedule.

This new technique is markedly different than traditional SEOP polarized ^{3}He targets utilized at JLab, and they should be seen as a complementary techniques with different strengths and challenges. The most important distinction in our context is that SEOP becomes less effective at high magnetic fields due to increasing wall relaxation [9], while this technique improves in high magnetic fields, reaching competitive polarizations and densities above 2 T. Historically, the key advantage of SEOP systems has been the gas pressures at which they can operate, while MEOP has provided faster pumping rates at much lower pressures [2]. At JLab, SEOP is typically performed in a high-temperature pumping cell at 10 bar and 473 K, creating gas densities of 10 amagats in the room temperature target cell. Our technique aims to create a target cell density of roughly 5 amagats using 100 mbar gas at 5 K. Operating at subatmospheric pressures and cryogenic temperatures, our MEOP technique will require 4 layers of aluminum between scattered particles and the detectors (a flow diverter, target cell wall, heat shield and outer vacuum chamber), which we anticipate will result in a total aluminum thickness of roughly 0.75 mm. SEOP target cells have roughly 1.5 mm thick glass walls, and do not require any further chambers. Because SEOP cells are glass containing high pressure gas, pressure hazards must be considered. SEOP remains a vital tool for high luminosity polarized scattering experiments; our technique will be invaluable for applications, like CLAS12, where SEOP is not feasible.

C. Transverse Polarized ^{3}He Target

While this proposal focuses on longitudinally polarized scattering, we are investigating a concept to use this new target design to provide polarization transverse to the incident direction of the beam using superconducting shielding. Taking advantage of the progress of fellow Jefferson Lab scientists from the HD-Ice group, we will adapt their plan to cancel the CLAS12 solenoidal field and produce a transverse holding field with bulk, superconducting MgB_2 [20]. Our concept would polarize in CLAS12's 5 T field at 100 mbar, and transfer into

the target cell, held within the MgB_2 shield. Polarized ^{3}He requires only a small ($\sim$ 50G) holding field to maintain polarization, much less than the 1.5 T planned for HD-Ice. In our scheme, the longitudinally polarized ^{3}He spins will rotate adiabatically in transit, following a rotating field trapped into the bulk superconductor, arriving transversely aligned to the beam at the target cell. Simulations of the fields involved will inform our creation of a set of transit and holding field magnet coils, which will be used to lock the magnetic field into the bulk superconducting shield. The value of transversely polarized physics in CLAS12 would be immense, and further research into target methods is needed to realize it. Our concept for a transverse target is still in development, and the full approval of the high-impact rated proposal to utilize the HD-Ice transverse target is pending the successful demonstration of target methods.

D. Target Development

A working prototype of this new type of polarized target is being planned to assess the performance of the technique in experimental conditions. The target development will be a collaborative effort centered at JLab and led by J. Maxwell, with support from the Jefferson Lab target group, Hall B technical staff, and R. Milner's group at the Laboratory for Nuclear Science at MIT. The principle equipment required for the planned prototype are a 5 T warm-bore magnet, pumping and probe laser systems, a pulse tube cryocooler, a cryostat, and a vacuum pump system. A laboratory space at JLab that can accommodate both the laser and cryogenic systems will be necessary. The prototype will be tested in stages as it is assembled, allowing for tests of high-field MEOP at room temperature while the cryostat, built closely to the design of the Hall D cryotarget, is fabricated. The finished prototype will be used to confirm and expand the ENS results of achievable steady-state polarization, pumping rates and relaxation times for high-field MEOP, as well as assess our estimates of the rate of gas transmission between the cells. These results will inform our selection of pressure, polarization and beam current to maximize the figure of merit of the experiment. A focal point of the prototype testing will be in-beam studies at JLab's Upgrade Injector Test Facility to confirm the predicted suppression of the depolarization rate from diatomic helium due to the high magnetic field. We anticipate significant publishable results from the target development alone. Funding to support this course of study is being pursued through

the DOE's Early Career Award program, and through JLab's LDRD program.

IV. INCLUSIVE AND SEMI-INCLUSIVE DIS

A. Introduction

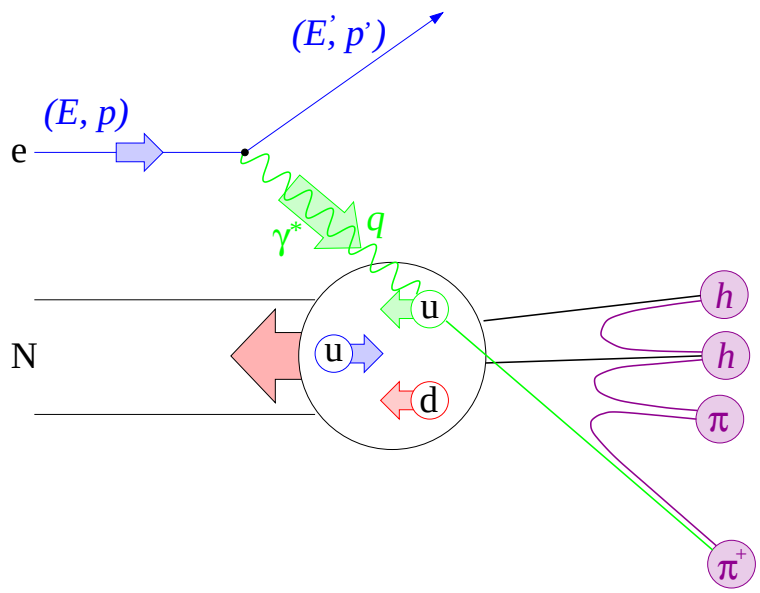

FIG. 5: Feynman diagram for semi-inclusive DIS [21].

The transition from a simple, one dimensional description using collinear parton distributions that depend on the nucleon's longitudinal momentum fraction, x, to a more complex nucleon picture with interacting and orbiting quarks, leads to a generalization of parton distributions, which include also the transverse parton momentum, k_T, and to the introduction of Transverse Momentum Dependent (TMD) parton distributions. SIDIS provides access to TMD parton distributions through measurements of spin and azimuthal asymmetries. The SIDIS reaction

$$\ell(k) + N(P) \to \ell'(k') + h(P_h) + X(P_X)$$

is such that a beam lepton ℓ with the 4-momentum k, scatters off of a target nucleon, N with 4-momentum P, and the scattered lepton ℓ' with 4-momentum k' is detected along with a single hadron, h, with 4-momentum P_h; all other produced particles in the final state, X, are not detected, see Fig. 5. Assuming a single photon exchange, the SIDIS cross-section, keeping only longitudinal polarization, can be decomposed into a sum of various azimuthal modulations coupled to corresponding structure functions. The SIDIS cross section has several contributions from different spin-dependent and spin-independent Structure Functions

(SFs) [22–24]:

$$\frac{d\sigma}{dxdydzdP_T^2d\phi_h} = \hat{\sigma}_U \Bigg\{ 1 + \varepsilon A_{UU}^{\cos 2\phi_h} \cos 2\phi_h + \sqrt{2\varepsilon\,(1+\varepsilon)} A_{UU}^{\cos\phi_h} \cos\phi_h$$
$$+ \lambda_\ell \sqrt{2\varepsilon\,(1-\varepsilon)} A_{LU}^{\sin\phi_h} \sin\phi_h$$
$$+ S_{||} \Big[\sqrt{2\varepsilon\,(1+\varepsilon)} A_{UL}^{\sin\phi_h} \sin\phi_h + \varepsilon A_{UL}^{\sin 2\phi_h} \sin 2\phi_h \Big]$$
$$+ S_{||} \lambda_\ell \Big[\sqrt{1-\varepsilon^2} A_{LL} + \sqrt{2\varepsilon\,(1-\varepsilon)} A_{LL}^{\cos\phi_h} \cos\phi_h \Big] \Bigg\} \tag{1}$$

where the asymmetries $A_{\dots}^{\dots}$ [24], which are defined by ratio of corresponding SFs to unpolarized SF, $F_{UU,T}$, depend on the kinematic variables x, Q^2, z, P_T and correspond to azimuthal modulations of the cross section in the azimuthal angle ϕ_h of the produced hadron, defined in the $\gamma^* N$ CM frame (see Fig. 6). The first and second subscripts denote respectively the lepton and target nucleon polarizations, while the superscript indicates the corresponding azimuthal modulation. Asymmetries are defined as ratios of corresponding polarized structure functions $F_{\dots}^{\dots}$ and unpolarized structure function F_{UU}. The unpolarized structure function, F_{UU}, or more precisely combination of structure functions corresponding to transverse and longitudinal polarization of the virtual photon $F_{UU,T} + \varepsilon F_{UU,L}$, is included in the definition of $\hat{\sigma}_U$. We use the usual SIDIS kinematic variables x, y, and z defined as: $x = Q^2/(2 \cdot P \cdot q)$, $y = (P \cdot q)/(P \cdot k)$, $z = (P_h \cdot P)/(P \cdot q)$, where $Q^2 = -q^2 = -(k - k')^2$ is the negative four-momentum squared of the virtual photon, and P_T is the transverse momentum of the detected hadron. The ratio ε of the longitudinal and transverse photon flux is given by: $\varepsilon = \frac{1-y-\gamma^2y^2/4}{1-y+y^2/2+\gamma^2y^2/4}$, where $\gamma = 2Mx/Q$, and M is the mass of the nucleon.

In the kinematic region, where the TMD description of SIDIS is appropriate, namely in the beam fragmentation region, $P_T/z \ll Q$, the transverse momentum of the produced hadron P_T is generated by intrinsic momenta of the parton in the nucleon $k_\perp$ and the transverse momentum of the produced hadron with respect to the fragmenting parton $\mathbf{p}_T$, such that the structure functions become convolutions of TMD parton distribution functions (PDFs), and TMD fragmentation functions (FFs). The convolution integral, for a given combination of TMD PDF f and FF D reads [24]

$$\mathcal{C}[wfD] = x \sum_q e_q^2 \int d^2k_\perp\, d^2\mathbf{p}_T \delta^{(2)}(\mathbf{p}_T + z\mathbf{k}_\perp - \mathbf{P_T}) w(k_\perp, \mathbf{p}_T) f^q(x, k_T^2) D^q(z, P_T^2), \tag{2}$$

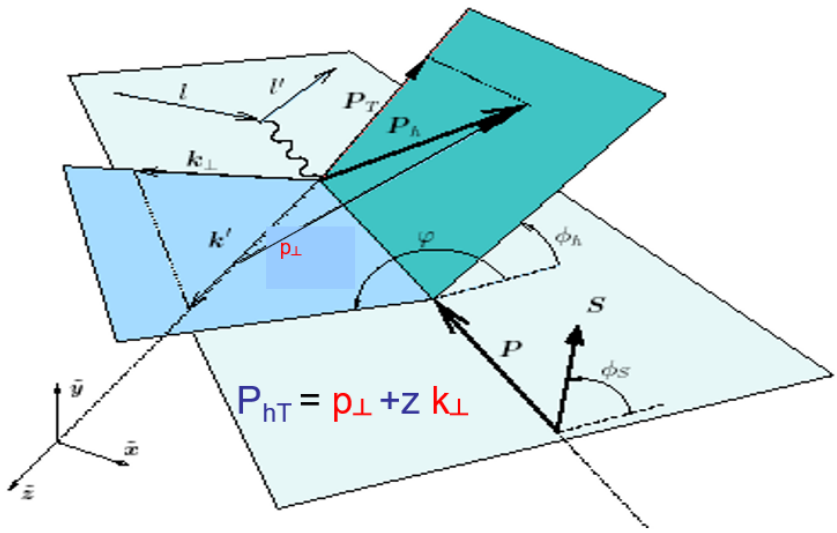

FIG. 6: SIDIS kinematical plane.

where w is a kinematical factor, and the sum is over all flavors of quarks and anti-quarks. The well-known SIDIS structure functions $F_{UU,T}$ and F_{LL} will be, thus, described by convolutions of f_1 and g_1 TMD PDFs and D_1 the unpolarized TMD fragmentation function, with $F_{UU,T} = \mathcal{C}\left[f_1 D_1\right]$, and $F_{LL} = \mathcal{C}\left[g_1 D_1\right]$(see Eq. 2).

Apart from the Q^2 dependence of the elementary lepton-quark cross section $\propto Q^{-4}$, some structures considered as higher twist functions appear in the cross section suppressed by an additional power of the hard scale Q. Higher twist structure functions will include convolutions of higher twist TMD functions. The leading and higher twist non-perturbative functions describe various spin-spin and spin-orbit correlations as corresponding operators include additional gluon and/or quark fields in the matrix element. In this proposal the main focus will be on the leading twist observables, related to F_{LL}, and $F_{UL}^{\sin 2\phi}$, but all other SFs, represented by different azimuthal moments will be measured, and can certainly contribute in better understanding of uderlying quark-gluon dynamics.

Measurements of flavor asymmetries in sea quark distributions performed in DY experiments, indicate very significant non-perturbative effects at large Bjorken-x, where the valence quarks are relevant [25]. In perturbative QCD, $q\bar{q}$ pairs are created from the gluon splitting. Since the masses of u and d quarks are small, the gluon splitting is not expected to generate quark flavor asymmetries. Older measurements by NMC [26] indicated that the integrated $\bar{d}$ distribution is larger than the integrated $\bar{u}$ distribution. The measurements by

the E866 collaboration [27], and more recently by SeaQuest [28], suggest that the $\bar{d}$ distribution is significantly larger than the $\bar{u}$ distribution in the full accessible x-range of proposed measurement ($x > 0.06$). The non-perturbative $q\bar{q}$ pairs are also correlated with spins and will most likely play a crucial role in spin-orbit correlations, and in particular, in single-spin asymmetries, that have been measured by various experiments in the last few decades.

B. Transverse Momentum Dependence

One of the most important questions concerning the 3D structure of the nucleon is the transverse momentum dependence of partonic distributions and fragmentation functions and the flavor and spin dependence of those functions. For precision studies of TMDs it is also important to understand the role of the medium, and the effects of in-medium modifications of the TMDs. This is crucial, since both COMPASS and JLab use nuclear targets to study polarization effects. Combination of different polarized targets (3He, NH_3, ND_3), will be important to sort out different contributions, in particular for large P_T region, which is one of the main goals of proposed measurement. Another important question to address is the role of exclusive processes in studies of SIDIS. To extract the distribution functions and thus details of the dynamics of quarks and gluons from SIDIS data, one also has to have a good understanding of the fragmentation process in which quark fragments into an observed hadron. Understanding of contributions of vector mesons (VMs) in general, and exclusive production of VMs in particular, will be important for interpretation of SIDIS observables. Here again, the combination of measurements with different targets will be important to quantify the systematics from different contributions, which are not accounted in the mainstream SIDIS analysis.

At Jefferson Lab, three of four halls are involved in 3D structure studies [29] including the HMS and Super HMS at Hall C [30–32], the BigBite and Super BigBite, as well as the SoLID detector at Hall A [33–35], and CLAS12 at Hall-B [36, 37]. Several experiments are already approved to study in detail the azimuthal modulations in SIDIS for different hadron types, targets, and polarizations in a broad kinematic range [31, 33–39]. The larger acceptance coverage of the CLAS12 detector allows measurements over a wide range of P_T (up to 1.5 GeV), and Q^2 (up to 10 GeV^2), while the SoLID detector would allow measurements of all kind of polarization asymmetries at large x with superior precision.

The most prominent leading twist observable is the ϕ_h-integrated cross section described by the F_{UU} structure function. In the TMD formalism, the final hadron $\mathbf{P}_T$ results from the initial quark $k_\perp$ and the fragmenting quark $\mathbf{p}_T$ and up to order $\mathcal{O}(k_T/Q)$ the momentum conservation gives $\mathbf{P}_T = zk_\perp + \mathbf{p}_T$. The structure function F_{UU} is given by the convolution integral $\mathcal{C}[f_1 D_1]$: Collinear PDFs have flavor dependence, thus it is not unexpected that also the transverse momentum dependence may be different for the different flavors [40]. Model calculations of the transverse momentum dependence of the TMDs [41–44] and lattice QCD results [45, 46] suggest that the dependence of the widths of the TMDs on the quark polarization and flavor may be significant. It was found, in particular, that the average transverse momentum of antiquarks is considerably larger than that of quarks [47, 48]. The frequently used assumption of factorization of x and k_T (or z and P_T) dependencies [49] may be significantly violated (see Fig. 10 of [50]). For instance, the predicted average transverse momentum square $\langle k_T \rangle$ of quarks and antiquarks may depend strongly on their longitudinal momentum fraction x within the framework of the chiral quark soliton model [47].

The first observation of a Single Spin Asymmetry (SSA) in SIDIS pion electroproduction was made by HERMES [51] in an attempt to access the distributions of transversely polarized quarks in the longitudinally polarized nucleon, $h_{1L}^\perp$. The physics of $F_{UL}^{\sin 2\phi}$, which involves the Collins fragmentation function $H_1^\perp$ and Mulders distribution function $h_{1L}^\perp$, was first discussed by Kotzinian and Mulders in 1996 [22, 23, 52].

$$F_{UL}^{\sin 2\phi_{\rm h}}(x, z, P_T) = \mathcal{C}\left[\frac{2(\hat{h}\cdot k_\perp)(\hat{h}\cdot \mathbf{p}_T) - (\mathbf{p}_T \cdot k_\perp)}{zM_N m_h} h_{1L}^\perp(x, k_T^2) H_1^\perp(z, P_T^2)\right] .$$

The same distribution function is accessible, in particular, in double polarized Drell-Yan, where it gives rise to the $\cos 2\phi$ azimuthal moment in the cross section [53]. The behavior of the Mulders distribution function was subsequently studied in many models, including the large-x [54] and large N_c [55] limits of QCD.

Measurements of the $\sin 2\phi$ SSA [52], allows the study of the Collins effect with no contamination from other mechanisms. A measurably large asymmetry has been predicted only at large x ($x > 0.2$), a region well-covered by JLab [56]. The existing data indeed indicate that at large x the F_{UL} may be significant [57–59]. In Fig. 7 the latest COMPASS measurements [58–60] are compared with $D(y)$-rescaled HERMES points [51] and model predictions

for COMPASS kinematics [61], indicating that there may be some tension between negative hadron SIDIS measurements at large x with HERMES [51], and in particular with JLab.

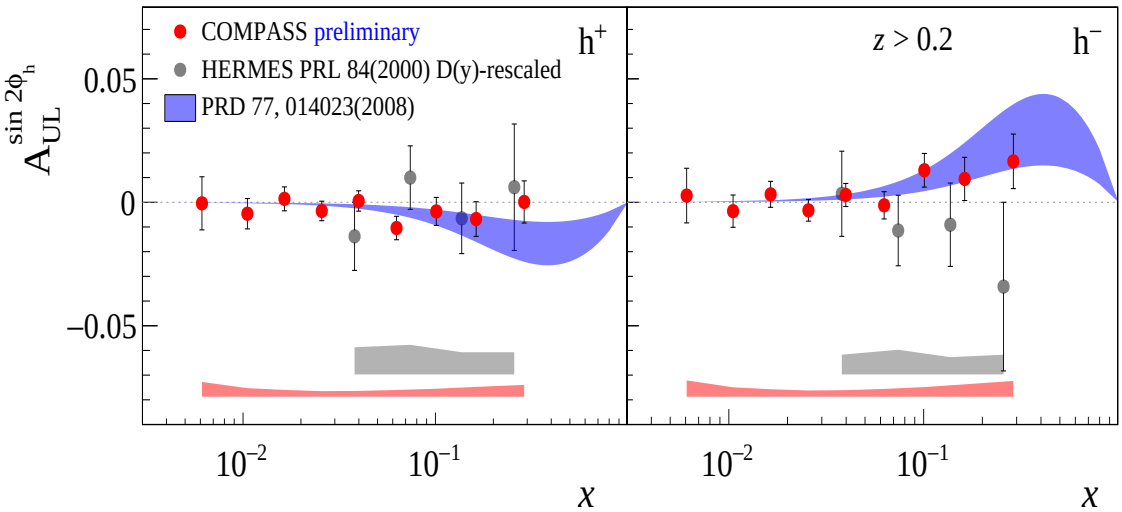

FIG. 7: The $A_{UL}^{\sin(2\phi)}$ results obtained by HERMES [51] and preliminary results by COMPASS [58, 59] and available model predictions [61].

There have been many studies dedicated to model calculations of TMDs, see for example [41, 62–76]. In addition, very exciting results of TMDs have come from lattice QCD calculations [45, 46, 77], indicating, for instance, that spin-orbit correlations could change the transverse momentum distributions of partons. Lattice calculations suggested that transverse momentum distributions depend both on flavor and the spin orientation of quarks (see Fig. 8). Measurements of the P_T-dependence of the double spin asymmetry (DSA) A_1, performed at JLab, with longitudinally polarized NH_3 target [57], suggest that the widths of parton distributions may indeed depend on the spin orientation. The P_T-dependence of the A_1 DSA for positive and negative hadron productions measured recently by COMPASS [58, 59] and HERMES [78] appeared to be well compatible with a constant function. This could indicate that transverse momentum widths of g_1 and f_1 are the same [43] in the kinematics not dominated by valence quarks. The possible correlation between the x and P_T of the hadron is one of the important issues to address by experiment. Such correlations tend to be much weaker for neutral pions.

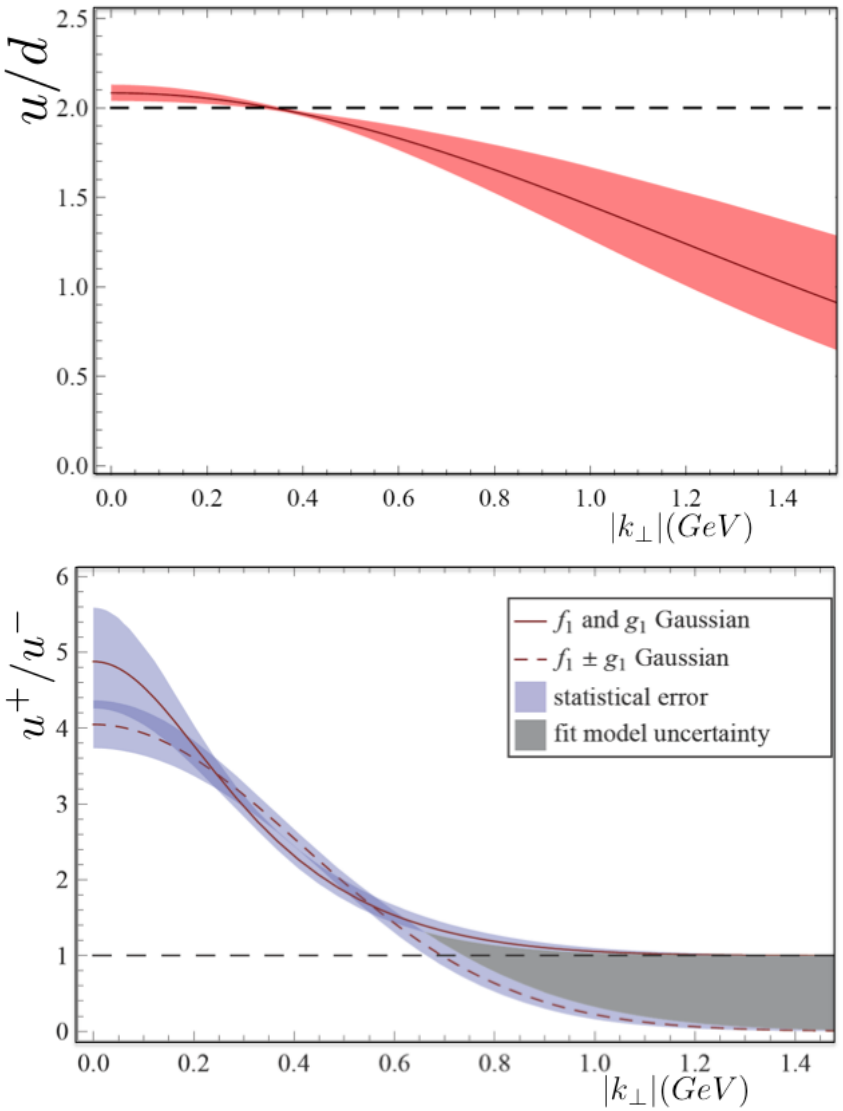

FIG. 8: Lattice calculations for k_T-dependence of ratios of u/d quark distributions (upper) and u^+/u^--distributions (lower) [46].

C. Nuclear Corrections to SIDIS

The SIDIS process for a nucleon in a light nucleus, e.g. the deuteron and ^{3}He, is theoretically most straightforwardly described as PWIA on the struck nucleon and the effects of the spectator nucleons are described by a convolution model. In this simplest approximation, the nuclear corrections for SIDIS are taken to be the same as for inclusive DIS.

However, there are nuclear-dependent corrections to to this picture. For example, the final-state interaction (FSI) with the spectator nucleons can be significant. The relative energy between the (A−1) system and the system of the detected pion and the remnant

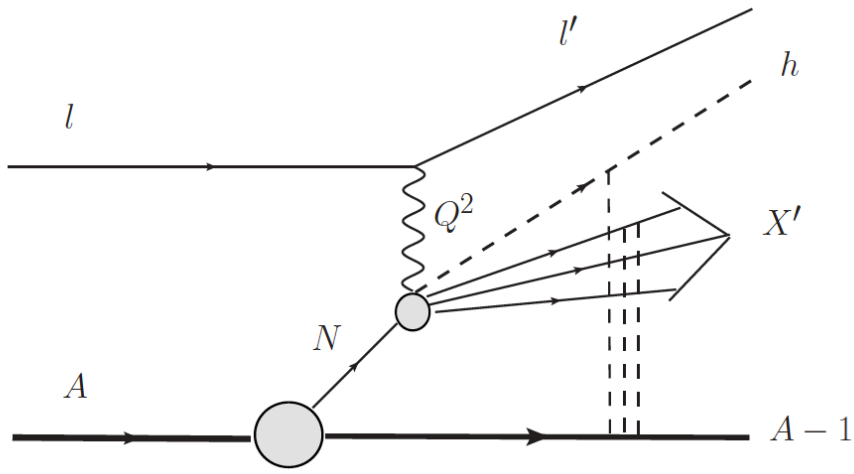

FIG. 9: Interaction between the (A−1) spectator system (fully interacting) and the debris produced by the absorption of a virtual photon by a nucleon in the nucleus.

(see Fig. 9) is a few GeV therefore the final-state interactions (FSI) can be treated within a generalized eikonal approximation framework (GEA). The GEA was already successfully applied to unpolarized SiDIS, and the distorted spin-dependent spectral function has been calculated [79] for the spectator SiDIS, where a slow (A−1) nucleon system, acting as a spectator of the photon-nucleon interaction, is detected, while the produced fast hadron is not.

The dilution factors and effective polarizations have been determined to differ by about 15% from the PWIA values. The effective polarizations occur in products with the dilution factors and to a large extent the product is close to the PWIA values [80]. However, a highly precise SIDIS data set on polarized ^{3}He, as proposed here, will provide a significantly more stringent test of the theoretical formalism.

The theory produces a distorted spin-dependent spectral function, which is dynamical and process dependent. For each experimental point in (x, Q^2), a different distorted spin-dependent spectra function has been calculated. With the proposed spin-dependent SIDIS data on the polarized ^{3}He target from CLAS12, the distorted spin-dependent spectral function cane be extracted and compared with theory.

It is obvious that having spin-dependent SIDIS data from both the deuteron (2 MeV weak binding) and ^{3}He (8 MeV binding) can constrain the theoretical understanding of the

nuclear corrections. Understanding the SIDIS nuclear corrections in light nuclei, where the ground state can be calculated precisely, is the launching point for understanding these important effects in heavy nuclei. The entire program of three-dimensional imaging rests on accurate determination of nucleon properties in the presence of dynamical nuclear effects.

Further, we point out that when one looks at this from the partonic view, we often use for interpretation of data a picture of electron-quark scattering convoluted with quark hadronization. Nuclear effects are typically, and naively, included as a convolution: of an EMC effect to electron-quark scattering and an attenuation representing the hadronization. This factorized approach is simplistic even for the free proton, and adding nuclear effects complicates it even more. This description does not hold.

In the SIDIS measurements proposed here, we have to consider a spin-dependent reaction on the simple ^{3}He nuclear system, which will have such nuclear effects. Thus, we can confront nuclear corrections not only at the cross section level but only with spin observables. This understanding is essential for making progress in the spin-dependent SIDIS/TMD program in general. We argue that our proposed measurements here on ^{3}He are needed in addition to those on the proton and deuteron if one is serious about understanding these essential nuclear corrections. Finally, the CLAS12 large acceptance and ability to detect the complete final-state (pions, kaons, recoil particles etc.) is absolutely unique.

D. Monte-Carlo Simulations of DIS and SIDIS from the Polarized ^{3}He Target

Detailed Monte-Carlo Simulations of DIS and SIDIS processes for ^{3}He target were performed using the full CLAS12 simulation and reconstruction chain. Events were generated with the CLAS version of the PEPSI [81] (LEPTO based) polarized SIDIS generator, digitized using the gemc (GEANT) and reconstructed with the latest available (v.6.5.3) clara/coatjava reconstruction framework.

We have chosen a logarithmic binning (see Appendix) that is consistent with considerations of the future EIC. The kinematics including large x and relatively low Q^2 covered by JLab will be accessible by the future Electron Ion Collider, EIC [82], only at very small y, providing critical complementary information for detailed TMD evolution studies. The relative coverage of CLAS12 (1 hour of running wih the polarized ^{3}He target) and different EIC configurations is shown in Fig. 10. The binning has been chosen to cover the full range

in x and Q^2 accessible by EIC and JLab12, relevant for studies of evolution of TMDs, in particular the Sivers TMD. The range in x with $x_{min} - x_{max}$ (0.005-0.99), and range in Q^2 with $Q^2_{min} - Q^2_{max}$(1-2500) (GeV/c)^2 were divided to N_x=60, and N_q=100 bins in log scale, respectively, with $x_i = x_{min}e^{i\Delta x}$ and $Q^2_i = Q^2_{min}e^{i\Delta Q^2}$, where

$$\Delta x = \ln(x_{max}/x_{min})/N_x \ , \tag{3}$$

$$\Delta Q^2 = \ln(Q^2_{max}/Q^2_{min})/N_q \ . \tag{4}$$

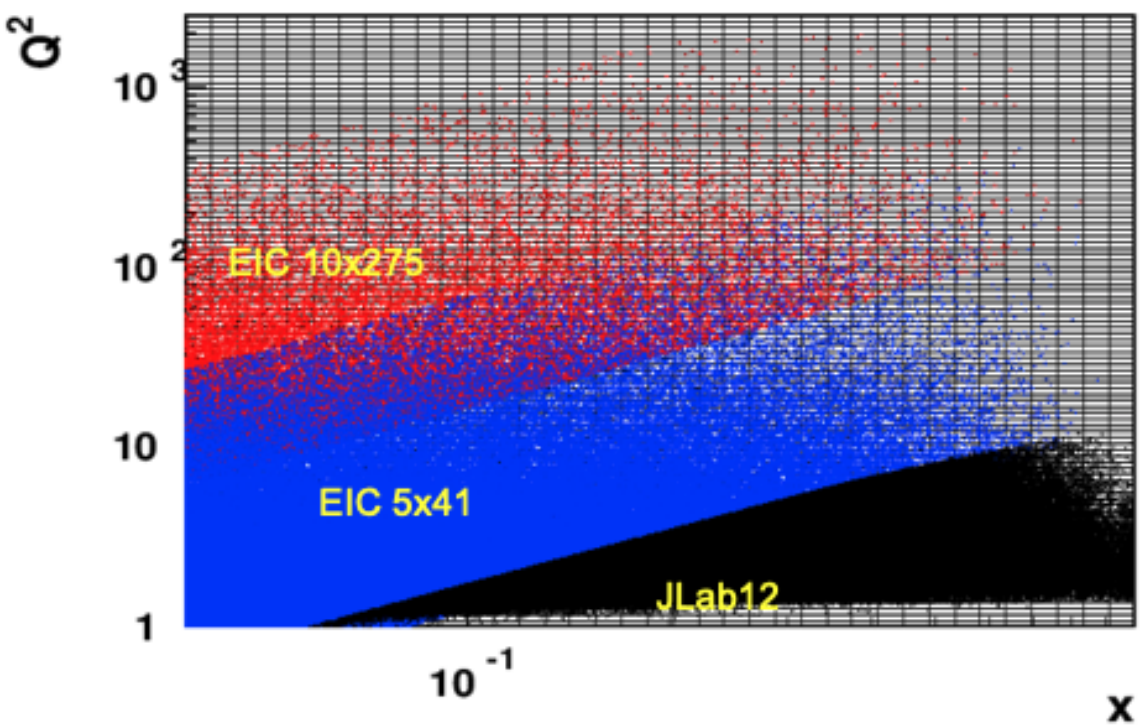

FIG. 10: The kinematic coverage in Q^2 (GeV/c)^2 and x of CLAS12 compared to different EIC configurations ($y_{min} > 0.015$).

The bin sizes are still significantly larger than the resolutions of CLAS12 in x and Q^2 by factors of 4 and 5, in the worst cases, respectively (see Fig. 11), as extracted from full MC reconstruction chain.

E. Inclusive Rate Estimation and Asymmetry Statistical Uncertainty Projection

The reconstructed events from the CLAS12 simulation were used as pseudo-data to estimate the rates and the projected statistical uncertainty in the asymmetry. The DIS rate

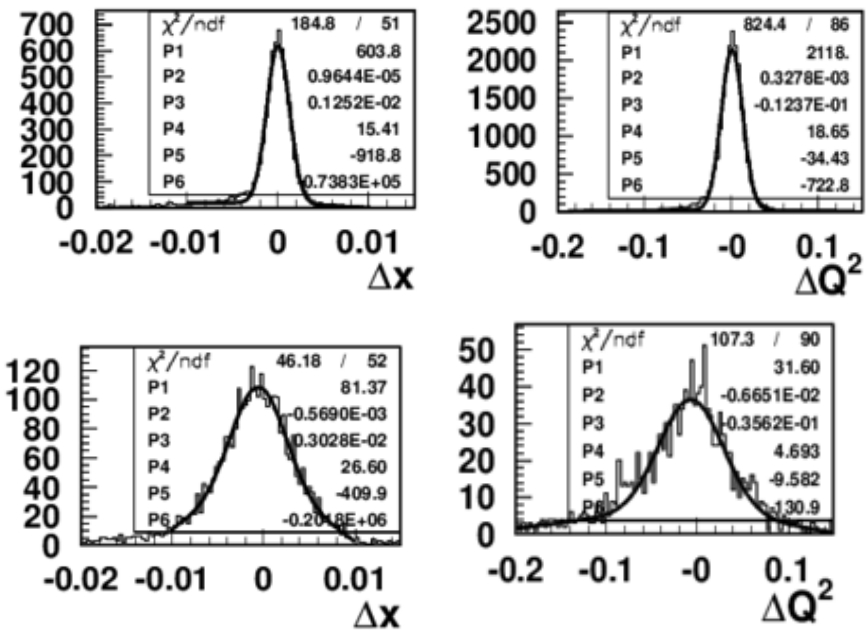

FIG. 11: Resolutions for CLAS12 x and Q^2, with upper row showing lowest x and Q^2 (in GeV^2) bins and lower row showing resolutions for highest accessible x and Q^2 bins, 0.003 and 0.04 (P3 in plots), respectively.

for ^{3}He was obtained by combining simulations for the proton and neutron separately, thus neglecting any nuclear effects. DIS events were selected by applying the cuts: $Q^2 > 1$ (GeV/c)^2 and $W^2 > 4$ (GeV/c)^2. The ^{3}He pseudo-data were sorted into the logarithmic bins described above. The number of events in each (x_B, Q^2) bin was determined and scaled to N corresponding to 30 PAC days of running. Then, the projected statistical uncertainty in the asymmetry for each bin of (x_B, Q^2) was determined using the formula

$$\delta A = \frac{1}{\sqrt{N} \cdot D \cdot P_t \cdot P_b} \ , \tag{5}$$

where N is number of counts for that given bin corresponding to 30 days of running and D is the dilution factor. The dilution factor for ^{3}He, has been studied using the MC samples for neutron and proton. The dilution factor was also studied using proper normalization of CLAS12 proton (RGA) and deuteron (RGB) data sets. Kinematical dependences of dilution factors from data and MC were found to be consistent with each other within a few percent (see Fig. 12). We note that data taking on $A_n^1(x, Q^2)$ in Hall C is in progress over the kinematic range $0.3 < x < 0.77$ and $3 < Q^2 < 10$ (GeV/c)^2 - see Table IV in the Appendix.

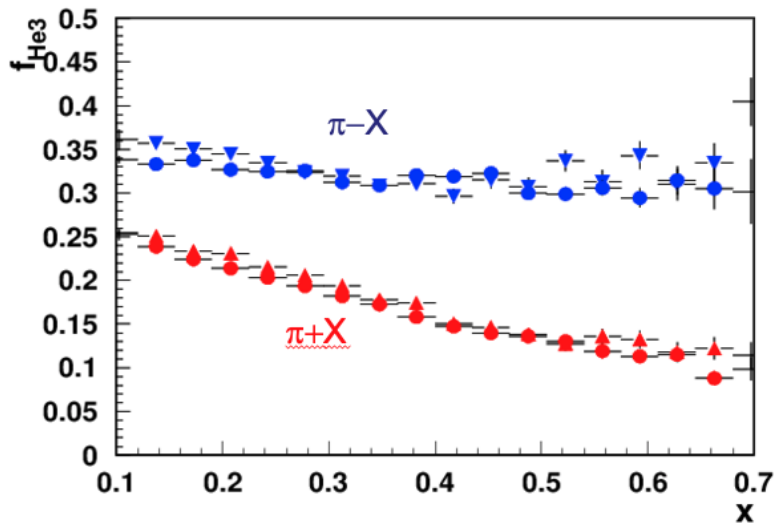

FIG. 12: x-dependence of dilution factors extracted from the combination of RGA and RGB data (circles) and MC (triangles) for semi-inclusive $\pi^{\pm}$ production.

For projections we have used $P_t = 0.5$ and $P_b = 0.8$ for the values of the target and beam polarization, respectively. Fig.13 shows the projected count and statistical uncertainty for 30 days run as function of Q^2 vs x_B. Fig. 14 shows the statistical uncertainty as a function of x_B for different bins of Q^2.

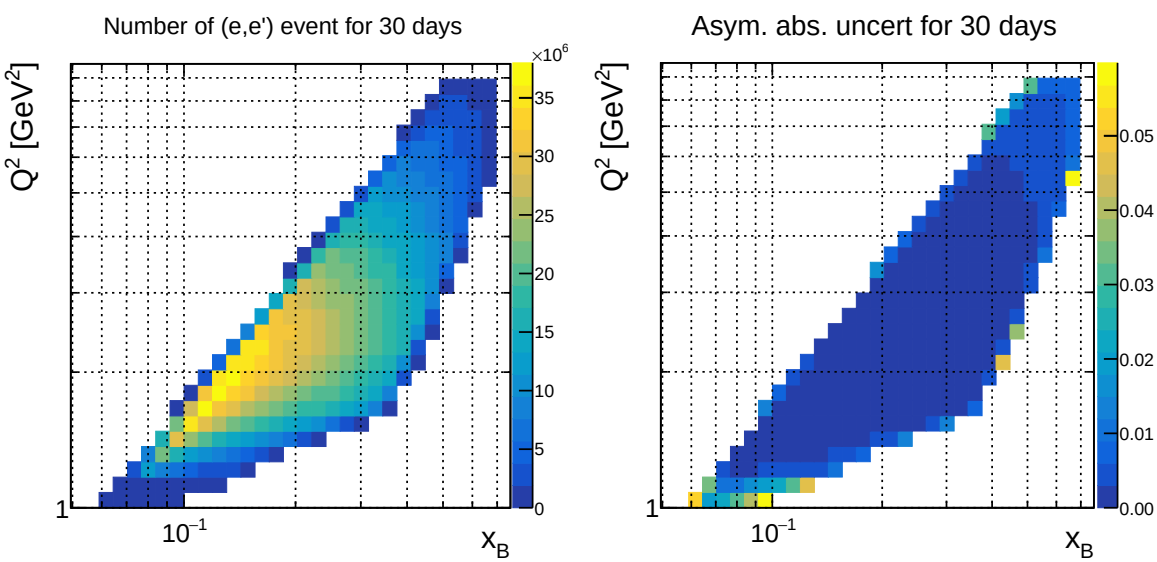

FIG. 13: Projected number of DIS events and absolute statistical uncertainty in the asymmetry for 30 days of running on the polarized ^{3}He target.

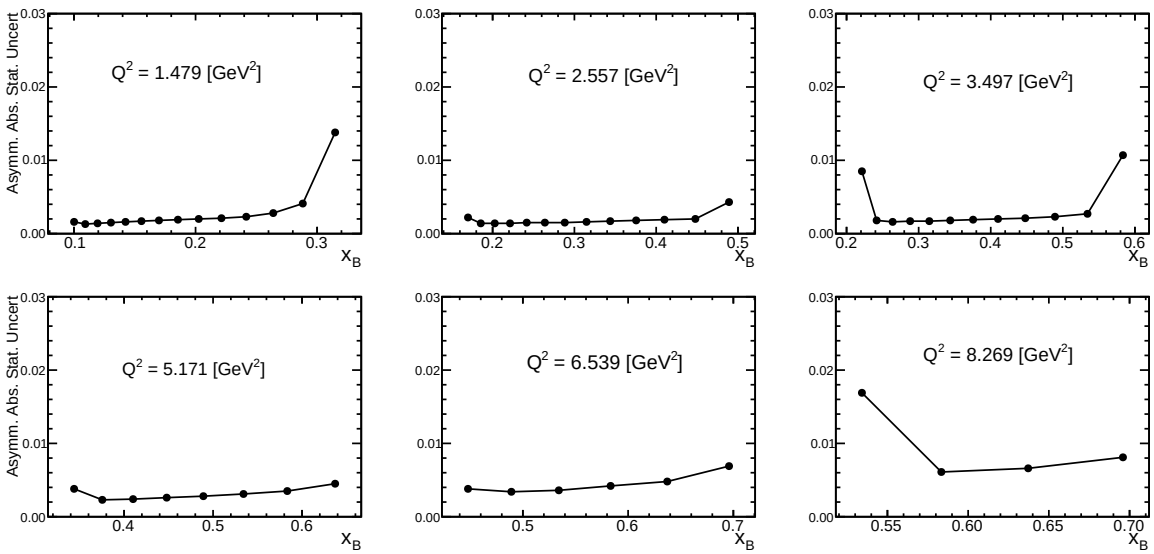

FIG. 14: Projected absolute statistical uncertainty in the asymmetry as a function of x_B for different Q^2 bins.

F. SIDIS: x and z Projections for Charged Pion Production in SIDIS

Fig. 15 shows the $x-$dependence projection plot for inclusive and SIDIS charged pion production. In this proposal, the cuts $Q^2 > 1$ (GeV/c)^2, $W^2 > 4$ (GeV/c)^2 and $y < 0.85$ are applied to select (e, e') DIS events. For SIDIS $(e, e'\pi^{+/-})$ the cut $z > 0.3$ is applied to ensure that the pions are leading (dominated by current fragmentation). The CLAS12 projected data points are for 30 days of running at the design luminosity. For comparison, the HERMES proton data from [83] are shown with the applied cuts: $Q^2 > 1$ GeV^2, $W^2 > 10$ GeV^2, $0.2 < z < 0.8$, $y < 0.8$ and $x_F > 0.1$.

Figs. 16 and 17 show the $z-$dependence projection plots. The same selection cuts as for Fig. 15 were used. We do this projection for two different x bins, the valence region $0.1 < x < 0.6$ and sea region $0.055 < x < 0.1$. We compare to the HERMES data on the proton in [86]. The curves use GRV [84] PDFs, and $D_1(z)$ from DSS [85].

G. Projection for the P_T dependence at different values of Q^2

Fig. 18 shows the projected statistical uncertainties for the 30 day run for the P_T-dependence of A_{LL} for the measured Q^2 of CLAS12 with an incident energy of 10.6 GeV. The Fig. 19 shows the projection for three Q^2 bins: $1 < Q^2 < 2$ (GeV/c)^2, $3 < Q^2 < 4$ (GeV/c)^2 and

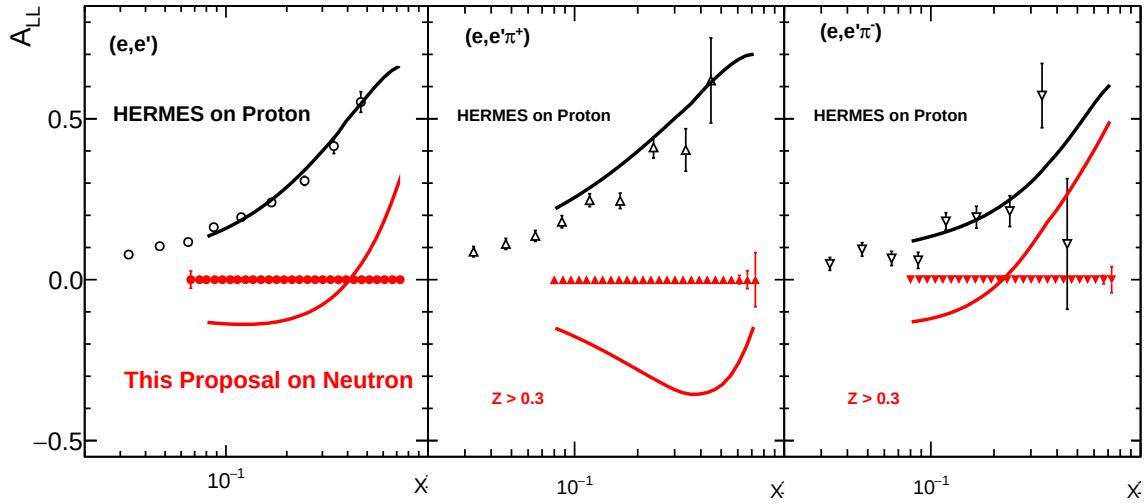

FIG. 15: $x-$dependence projection plot for charged pions, the black data points are HERMES data [83], the red data points are projection for this proposal. The curves use GRV [84] PDFs, and $D_1(z)$ from DSS [85], with black curves calculated for proton, and red curves calculated for neutron.

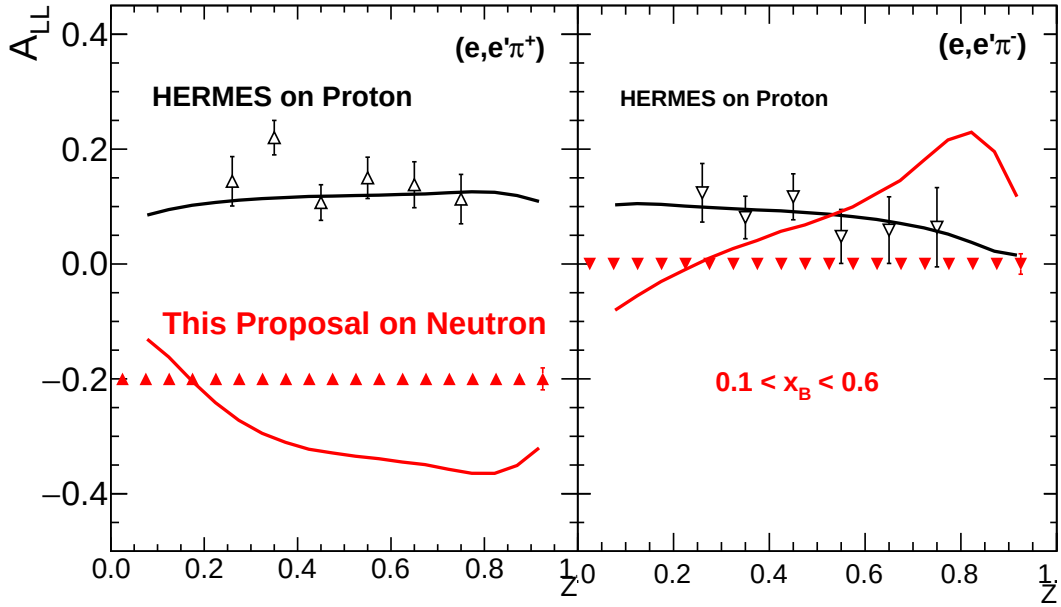

FIG. 16: $z-$dependence projection plot for charged pions in the valence region $0.1 < x < 0.6$, compared to the HERMES data on proton [86]. The curves use GRV [84] PDFs, and $D_1(z)$ from DSS [85].

$Q^2 > 5$ (GeV/c)^2. The theory curves in these figures are from [87].

The statistical precision of the proposed measurements at large x and in the large P_T range is much higher than that of HERMES and COMPASS [59] and comparable with pro-

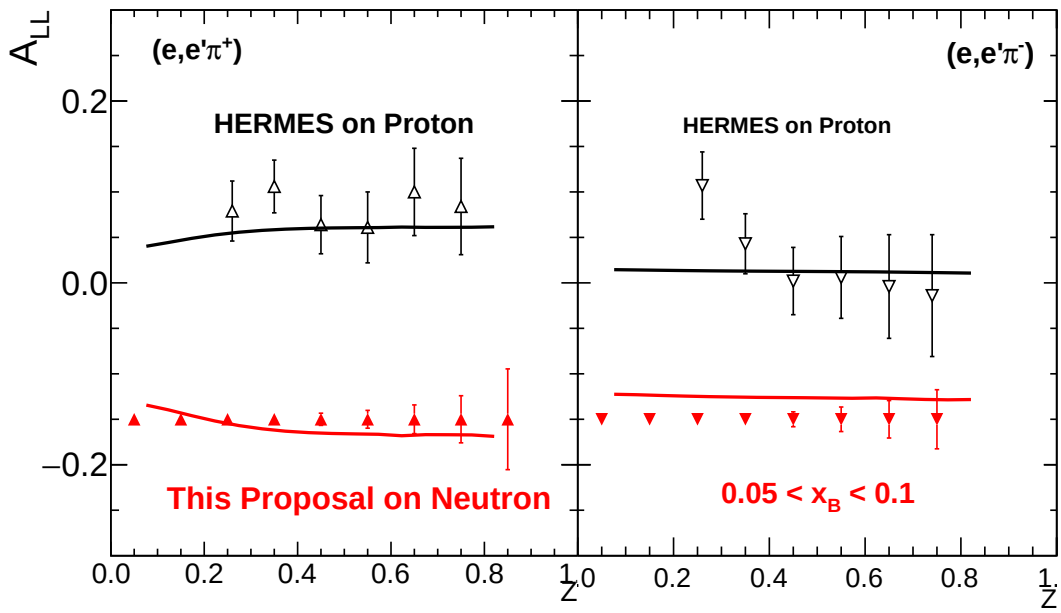

FIG. 17: $z-$dependence projection plot for charged pions in the sea region $0.05 < x < 0.1$, compared to the HERMES data on proton [86].The curves use GRV[84] PDFs, and $D_1(z)$ from DSS [85].

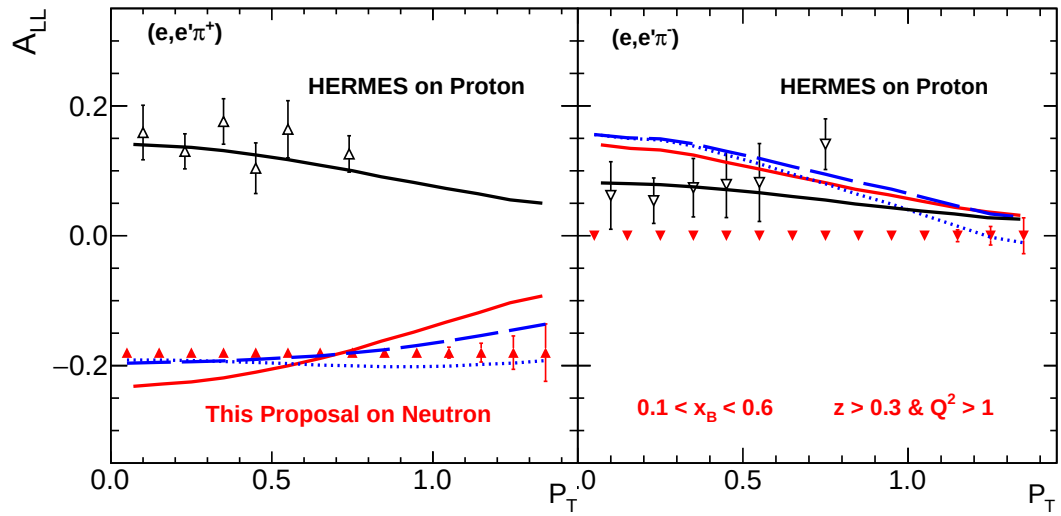

FIG. 18: Projected statistical uncertainties for the P_T-dependence of A_{LL} for the measured Q^2. The curves follow the approach in [43, 88, 89] with black and red curves calculated for $\langle p_\perp^2 \rangle = 0.16$, $\langle k_\perp^2 \rangle = 0.25$, for f_1 and 0.17 for g_1, for proton and neutron targets, respectively. The blue lines use Lattice calculations of widths of polarized and unpolarized u and d quarks [77], with dashed and dotted lines calculated assuming no flavor dependence, and with flavor dependence in k_T-distributions, respectively . More details available in Appendix F.

posed SoLID and CLAS12 ND_3 measurements, providing important complementary input to

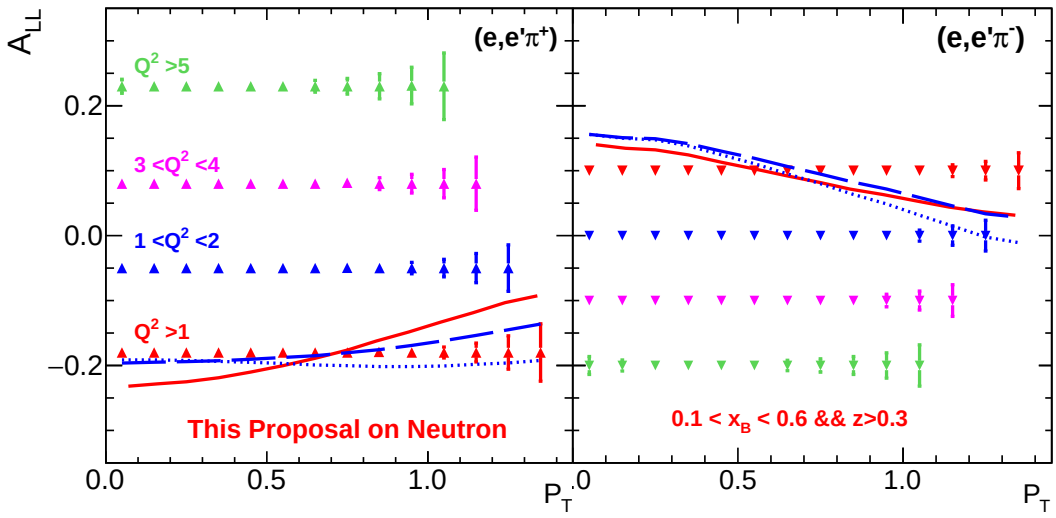

FIG. 19: This is the P_T-dependence projection for different bins in Q^2, see Fig. 18.

determine the k_T-dependence of the parton distribution functions from the P_T-dependence of A_{LL}. The prediction curves for asymmetry A_{LL} has been evaluated as a function of different kinematic variables using the well-known factorized Gaussian model approach as it was done in Ref. [43, 88]. For integrated PDFs (f_1 and g_1) and fragmentation function (D_1) a self-consistent choice of available grids was made selecting: GRV98(LO) [90], GRVS2000 [84] and [91] sets, correspondingly. The Gaussian width $\langle k_T^2 \rangle$ was set to 0.25 GeV^2 both for f_1 and g_1 and to 0.2 GeV^2 for D_1, which is the configuration that best describes preliminary COMPASS data [59].

We note that the theoretical predictions indicate that the neutron may have a stronger P_T dependence compared to that of the proton. Finally, the statistical precision of the proposed measurements is such that the Q^2 dependence of the P_T variation may be investigated experimentally to test the applicability of involved theory.

H. Comparison to CLAS12 Run Group C (E12-17-107) and proposed SoLID

1. *Comparison to CLAS12 on ND_3 Target*

While we regard the proposed measurements here on the polarized ^{3}He target as complementary to those approved on ND_3 (E12-07-107), it is instructive to compare the projected results. For ND_3, at high P_T, the dilution factor is much larger due to the presence of ex-

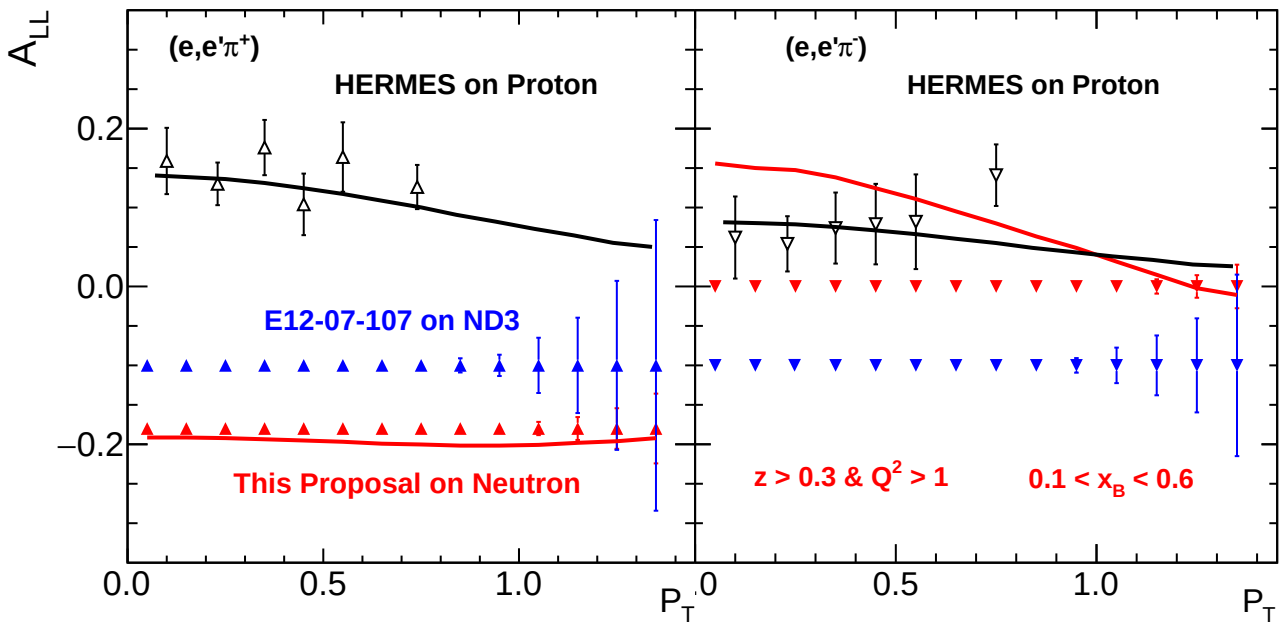

FIG. 20: Comparison of projected statistical uncertainties in A_{LL} for ND_3 (blue points) with the polarized ^{3}He target proposed here (red points).

traneous nuclei. Further, the proposed target polarization is only 30% as compared to 50% with the proposed polarized ^{3}He target. As seen from Fig. 20, for high P_T, the projected uncertainties for the polarized ^{3}He target here are significantly smaller.

2. *Comparison to the Proposed SoLID Detector*

The Solenoidal Large Intensity Detector (SoLID) is a proposed large acceptance detector system designed to pursue a diverse physics program, including 5 highly rated experiments covering PVDIS, SIDIS and J/ψ production. In its SIDIS configuration, SoLID will use high-pressure SEOP targets to provide longitudinal and transversely polarized ^{3}He targets. Table IV in Appendix E shows its capabilities for longitudinally polarized ^{3}He. For comparison we have made the following plots:

1. Q^2 coverage: Due to its larger acceptance, CLAS12 can reach to higher values of Q^2 with better statistical precision compared to SoLID, as seen in Fig. 21.

2. P_T coverage: Fig. 22 shows a comparison of projected statistical uncertainties vs. P_T for charged pions. At high P_T, the polarized ^{3}He proposal has better statistical precision, due to better acceptance for $P_T > 1.0$ (GeV/c), and extending to $P_T = 1.5$

(GeV/c).

3. Di-hadrons: Due to the larger acceptance for CLAS12, Fig. 23 shows that the polarized ^{3}He target proposed here will have a significantly higher yield of di-hadrons compared to the proposed SoLID.

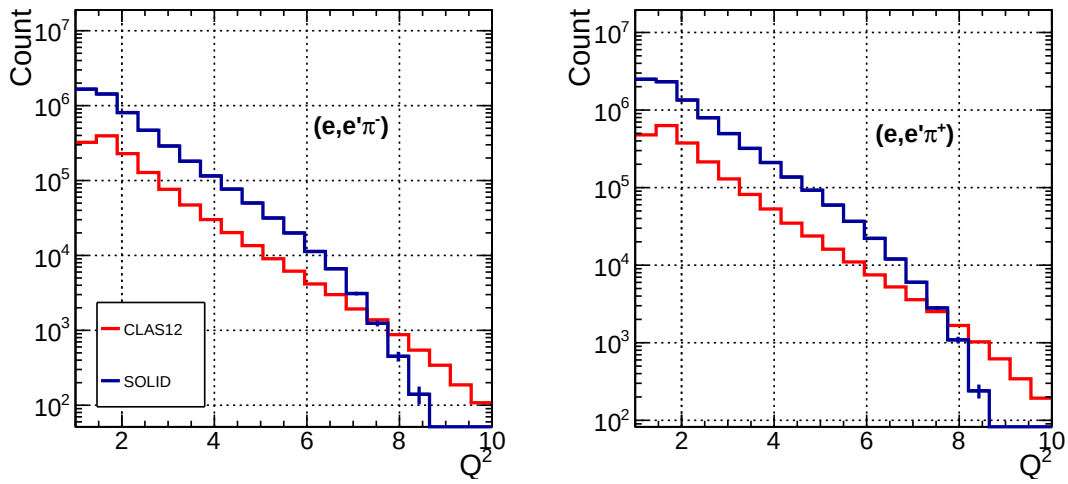

FIG. 21: Q^2 coverage for $(e, e'\pi^-)$ and $(e, e'\pi^+)$ for this proposal (red) and SoLID (blue).

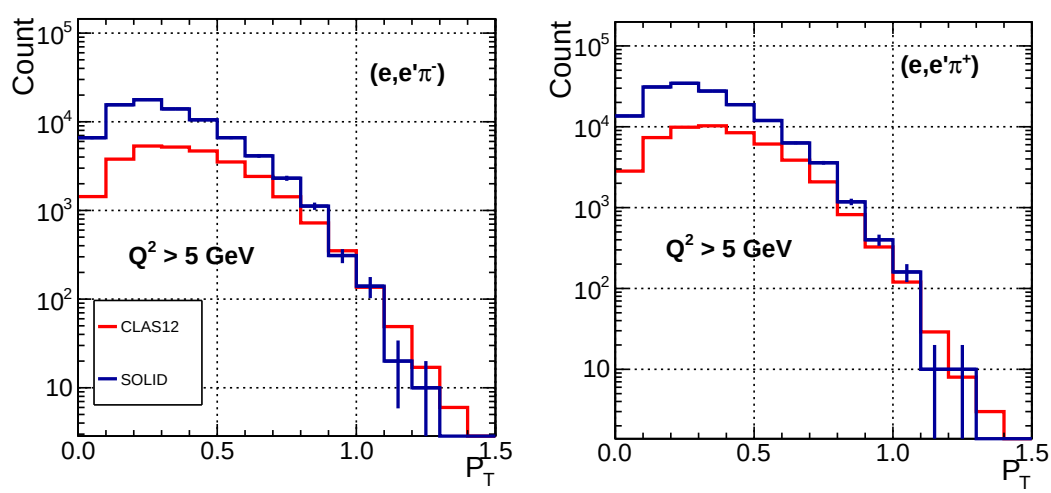

FIG. 22: P_T coverage for $(e, e'\pi^-)$ and $(e, e'\pi^+)$ for this proposal (red) and SoLID (blue).

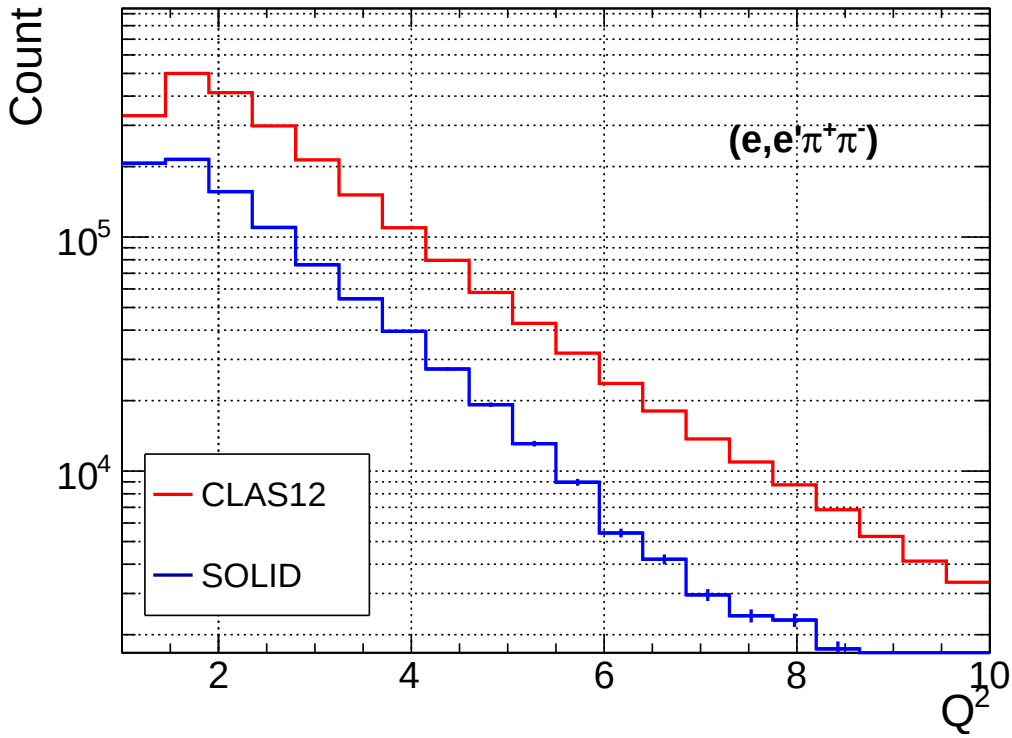

FIG. 23: Comparison of di-hadron yields from the polarized ^{3}He target (red) with those from SOLID (blue).

I. SIDIS: x, P_T and z Projections for Charged Kaons

Here, the event selection cuts are the same as for the pions. However, we relax the z cut to $z > 0.2$ to increase the statistics. Fig. 24 shows the projected plot for the charged kaon asymmetries as a function of x. Figs. 25 and 26 show the projected plots for the charged kaon asymmetries as a function of P_T for valence and sea quark regions. Figs. 27 and 28 show the projected plots for the charged kaon asymmetries as a function of z for valence and sea quark regions.

J. Measurements of Single Spin Asymmetries (SSAs) on the Polarized Neutron

The $\sin 2\phi$ moment of the single target spin asymmetry provides access to TMD $h_{1L}^{\perp}$ describing transversely polarized quarks in the longitudinally polarized nucleon, and Collins fragmentation function describing the hadronization of transversely polarized quarks. The Collins fragmentation functions for the favored and disfavored hadrons, is expected to have

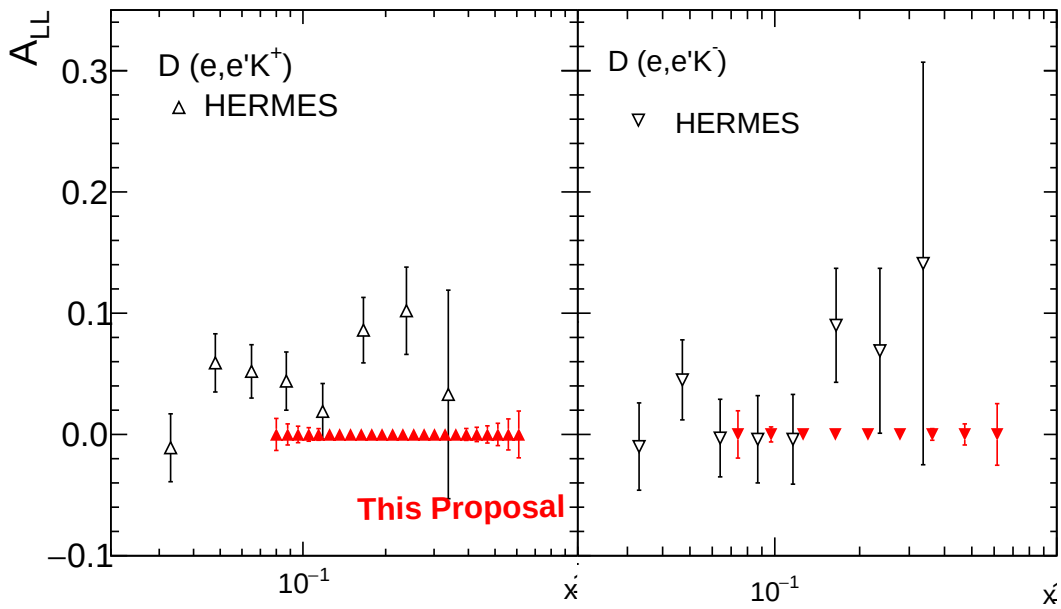

FIG. 24: $x-$dependence projection plot for charged kaon SIDIS asymmetry A_{LL}, compared to the HERMES data on deuterium [86].

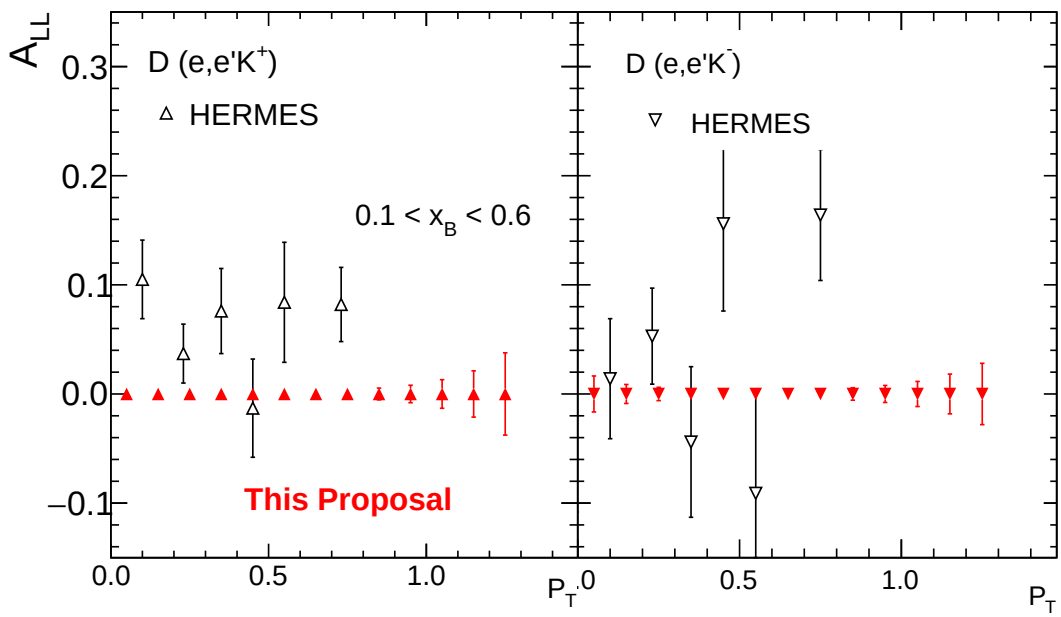

FIG. 25: P_T-dependence plots for charged kaons, compared to the HERMES data on Deuterium [86].

opposite signs, leading to prediction for significant differences in SSAs for positive and negative pions. Projections for x and z dependences of $A_{UL}^{\sin 2\phi}$ for 30 days of running with longitudinally polarized ^{3}He target are shown in Figs. 29,30. The asymmetry is expected to

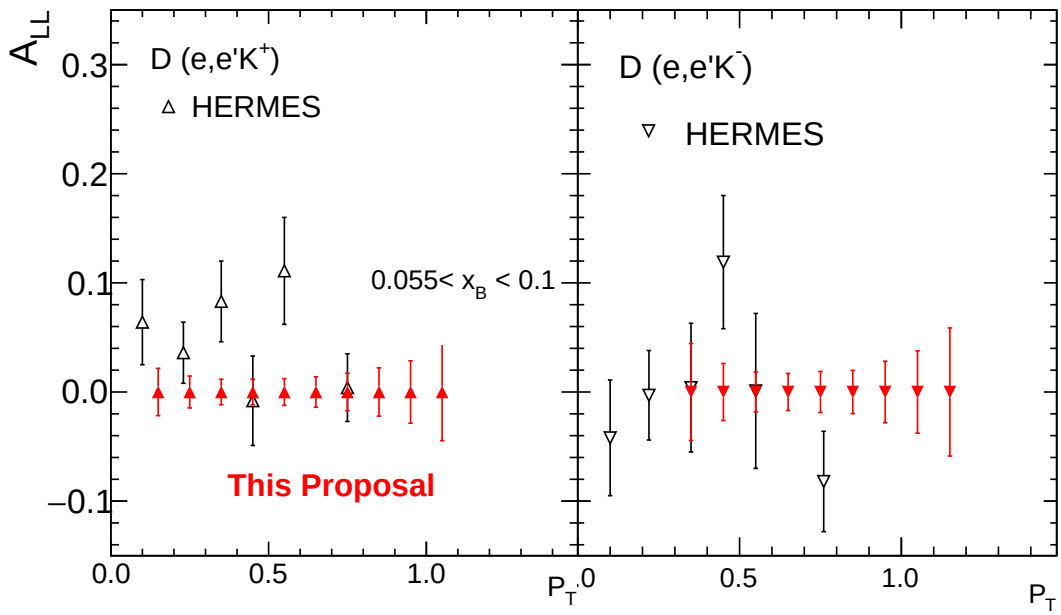

FIG. 26: P_T-dependence plots for charged kaons, compared to the HERMES data on Deuterium [86].

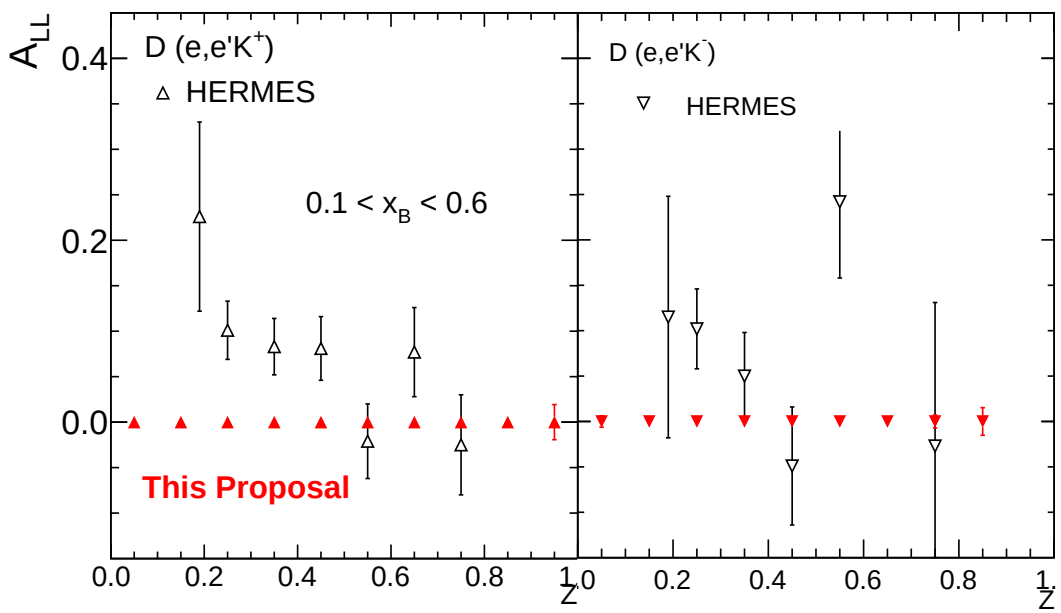

FIG. 27: $z-$dependence plots for charged kaons, compared to the HERMES data on Deuterium [86].

be sizable only at large x, z, and P_T, the kinematics well covered by CLAS12.

Theory predictions were calculated using the leading-order MSTW parametrizations [92] for the unpolarized PDF $f_1(x)$ and DSS [93] for the unpolarized fragmentation function

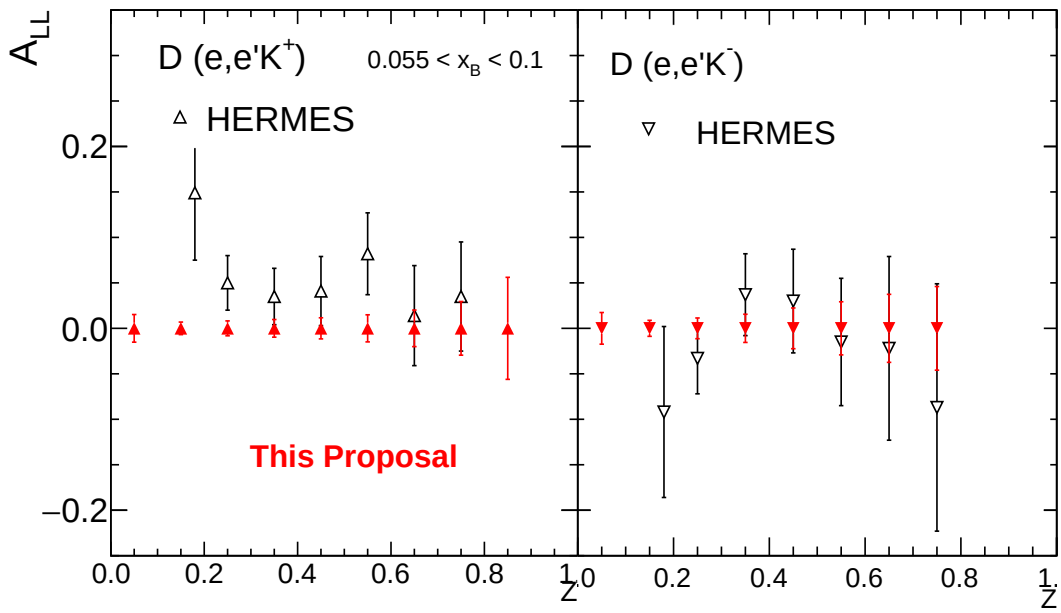

FIG. 28: P_T-dependence plots for charged kaons, compared to the HERMES data on Deuterium [86].

$D_1(z)$. In the calculations of $F_{UL}^{\sin 2\phi_h}$, the WW-type approximation is used to obtain the Kotzinian-Mulders function $h_{1L}^{\perp}(x)$ from transversity:

$$h_{1L}^{\perp(1)}(x) \approx -x^2 \int_x^1 \frac{dy}{y^2} h_1(y) \ .$$

For the transversity $h_1(x)$, and the Collins Fragmentation function $H_1^{\perp}(z)$, the parameterizations from Anselmino *et al.* [94], $f_1(x)$ from MSTW, $g_1(x)$ from GRV[84] and $D_1(z)$ from DSS [85] have been used (see appendix A.1 and A.4 in [89]). For the transverse momentum dependence of the TMD a Gaussians ansatz has been used with $k_{Tf_1}^2 = 0.25$ GeV^2, $k_{Tg_1}^2 = 0.19$ GeV^2 and $P_{TD_1}^2 = 0.2$ GeV^2.

K. Di-hadrons: $\overrightarrow{^3\mathrm{He}}(\vec{e}, e'\pi^+\pi^-)$

In addition to the single-hadron in the final state, as discussed in the previous sections, large acceptance of CLAS12 allows detection of multiparticle states, including pairs of hadrons in the final state [95, 96] detected in coincidence with the DIS electron. The invariant mass distributions of di-hadrons from different SIDIS and e+e- experiments indicate, the fraction of pions from vector meson (VM) decays may be very significant. Preliminary

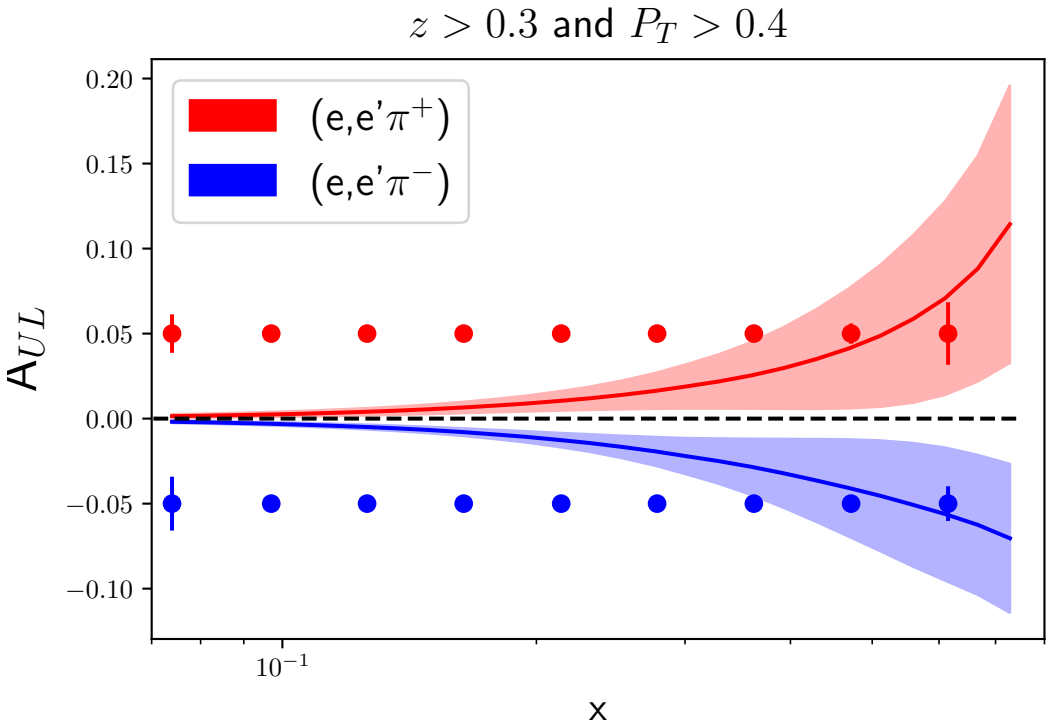

FIG. 29: Projection for x-dependence of $A_{UL}^{\sin 2\phi}$. Curves calculated using the MSTW parametrizations for the $f_1(x)$ [92], DSS [93] for $D_1(z)$, and the Collins function from Anselmino *et al.* [94].

CLAS12 data supports predictions from different LUND fragmentation based MCs, of very significant fraction of inclusive pions coming from correlated di-hadrons. The observables for pions from decays of vector mesons have peculiar spin and momentum dependences and may require different radiative corrections, modeling, and interpretation of observables sensitive to transverse momentum of quarks [97]. That makes studies of correlated semi-inclusive and exclusive di-hadrons in general, and rho mesons, in particular, crucial for interpretation of single-hadron measurements in SIDIS [97, 98].

Due to the additional degrees of freedom, usually encoded in the difference vector $\vec{R}$ between the two pions, di-hadron fragmentation allows a more targeted access to some aspects of the proton structure. In particular, the collinear twist-3 PDFs h_L and e can be accessed. They are two of the three collinear PDFs needed to describe the nucleon at twist-3, i.e. including gluon exchange with the scattered quark. In the single hadron case, these functions appear in the cross-section at twist-3 together with three other terms that are not known to be small. On the other hand, in the di-hadron case, the cross-section modulation

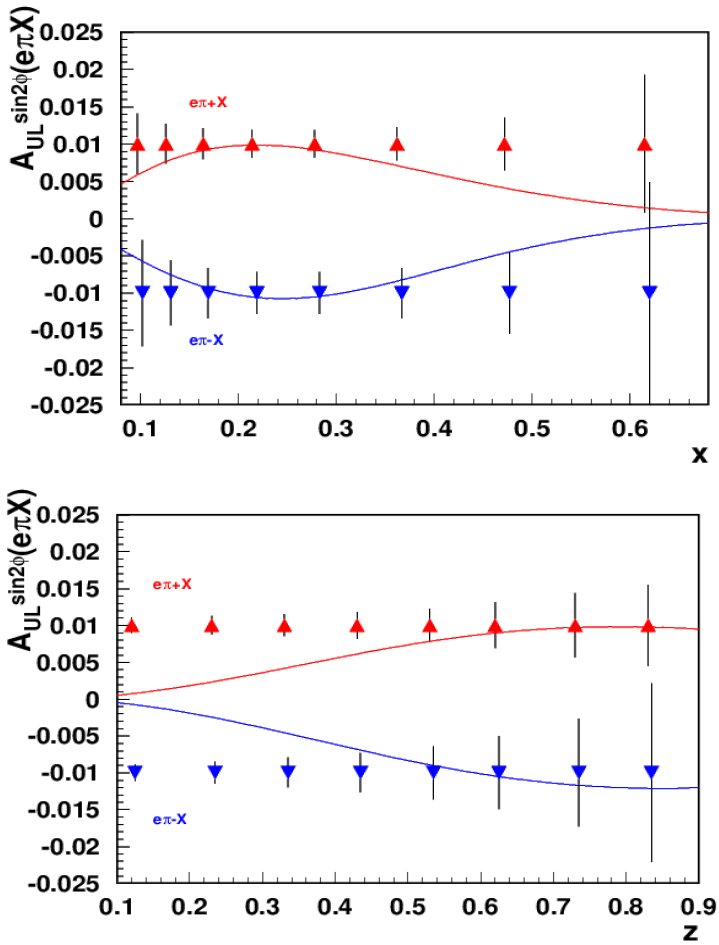

FIG. 30: Projections for $A_{UL}^{\sin(2\phi)}$ vs. x (top panel) and z (lower panel) for 30 days of running.

sensitive to h_L and e at twist-3 only contains one other term, which can be argued to be small [99].

Furthermore, di-hadron correlations allow for fragmentation functions that do not exist for single hadrons. Here we are most interested in the di-hadron fragmention (DiFF) function $G_1^{\perp}$, describing the dependence of a pair of unpolarized hadrons on the helicity of the fragmenting quark. This function is not allowed in the single hadron case and can be seen as analogous to the production of polarized single hadrons, e.g. Λ fragmentation. In the di-hadron case, the relative angular momentum between the two hadrons plays the role of the Λ polarization. Preliminary CLAS12 results on beam spin asymmetries have shown for the first time that $G_1^{\perp}$ has a significant magnitude. Detailed model calculations for this function exist in the NJL model [100] allowing insight into spin-orbit correlations in fragmentation.

Following [101], the relevant structure functions sensitive to e and h_L can be written in a collinear picture at twist-3 as

$$F_{LU}^{\sin\phi_R} = -x\frac{|R|\sin\theta}{Q}\left[\frac{M}{M_h}\,x\,e^q(x)\,H_1^q\big(z,\cos\theta,M_h\big) + \frac{1}{z}\,f_1^q(x)\,\widetilde{G}^q\big(z,\cos\theta,M_h\big)\right], \quad (6)$$

$$F_{UL}^{\sin\phi_R} = -x\frac{|R|\sin\theta}{Q}\left[\frac{M}{M_h}\,x\,h_L^q(x)\,H_1^q\big(z,\cos\theta,M_h\big) + \frac{1}{z}\,g_1^q(x)\,\widetilde{G}^q\big(z,\cos\theta,M_h\big)\right]. \quad (7)$$

Here, M_h is the pair invariant mass, θ is the angle between the directions of the emission and of the pair momentum in the center-of-mass frame of the two hadrons, where the emission occurs back-to-back, H_1 is the transverse spin dependent DiFF and $\tilde{G}$ are twist-3 DiFFs [101]. The DiFF $G_1^\perp$ contributes at leading twist coupled to the PDF f_1 in A_{LU} and to the helicity distribution function g_1 in A_{UL}. Figure 31 shows the projected uncertainties for DiFF asymmetries with the proposed running configuration for an asymmetry estimated following some reasonable assumptions. Given model calculations of h_L [72, 102, 103] and the preliminary

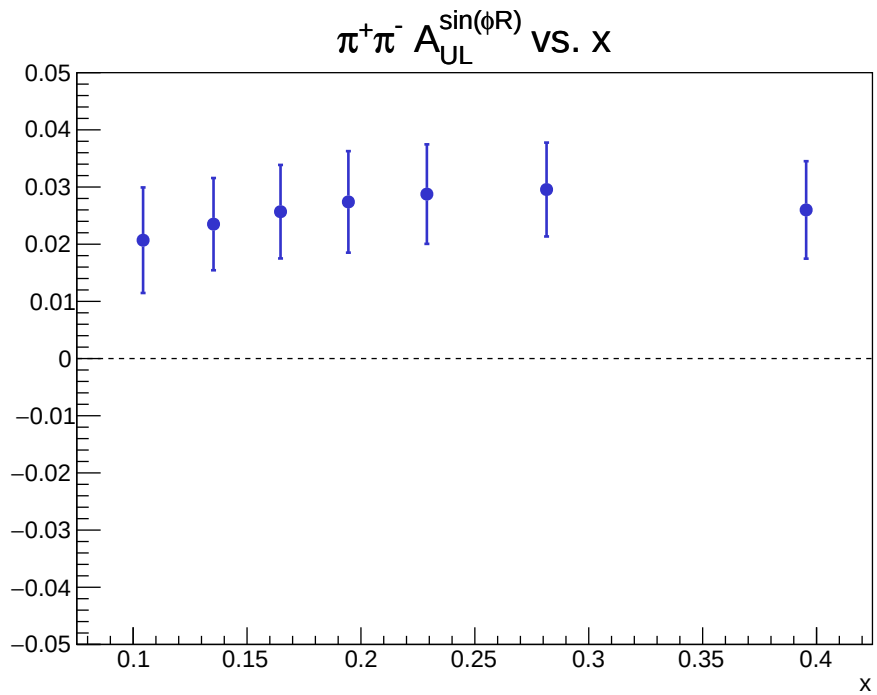

FIG. 31: Projections of the statistical uncertainties for $\pi^+\pi^-$ pairs for the proposed running time and conditions. The magnitude of the projected asymmetries is based on the observed magnitude of A_{LU} in CLAS12 data on a proton target, and on taking into account the relative size of e/h_L in a model calculation, as well as the isospin flip and the kinematic factors in the two measurements.

CLAS12 results sensitive to e and $G_1^\perp$, we expect signals of $\mathcal{O}(1\%)$, which are within the

reach of the measurement. Currently, the experimental information on these quantities is extremely limited. In addition to the preliminary CLAS6 results on h_L only a preliminary COMPASS measurement on the proton exists [104]. This reports small asymmetries, most likely due to sampling the function at small x. Therefore, the proposed polarized ^{3}He measurements will add valuable information on the flavor dependence of these functions, which are essentially unknown at the moment. Since e and h_L are connected to forces and force gradients, respectively on the scattered quark as it traverses the nucleon [105, 106], essential insight into nucleon structure can be gained.

L. Summary

Measurements with different targets and for different final states, including single and di-hadrons, provide important input for interpretation of systematic uncertainties of precision measurements in polarized SIDIS experiments, in particular at Jefferson Lab. Understanding the scale of contributions ($\sim M^2/Q^2$, $\sim P_T^2/Q^2$, target/current correlations, etc.) will define the limits on precision needed to separate various aspects of TMDs, such as evolution, higher twists, etc.

With expected strong medium modifications of the orbital structure of partonic motion, and corresponding transverse momentum distributions of partons in nuclei (NH_3, ND_3), ^{3}He target measurements of hadronic distributions at large transverse momenta will provide important information complementary to that obtained from measurements on other targets on the 3D structure of partonic distributions, most importantly on polarized distributions. Providing vital complementary information on partonic structure, di-hadron production is also crucial for the interpretation of single hadron SIDIS; CLAS12's large acceptance makes it best suited for measurements of di-hadrons in SIDIS.

V. SYSTEMATIC UNCERTAINTIES

While the statistical precision in the accessible kinematic region is unprecedented, systematic uncertainties must be considered.

A. Beam and Target Polarization Measurement and Reversal

The relative uncertainties on polarimetry are assumed to be 3% for the beam and 5% for the target. This gives a 3% relative uncertainty for A_{UL} measurements and a 6% relative uncertainty for A_{LL}. To reduce effects due to detector efficiency drift, we would plan to reverse the beam helicity at 30 Hz and the target polarization every 6 hours. This will result in 60 target spin pairs. Within a 6 hour target spin state, the detector efficiency will be monitored to a precision of 1% by the single electron/pion rate. The systematic uncertainty due to the detector efficiency drift may be estimated as $1\%/\sqrt{60} \sim 1 \times 10^{-3}$.

B. Random coincidences

With a 5 ns coincidence window, the average random coincidence background is ∼2% for both charged pion channels. The background will be further suppressed by a factor of ∼5 with the demand of a common vertex to vertex coincidence. On average, there will be <0.5% (relative) systematic uncertainty from background.

C. Nuclear Corrections

The ^{3}He scattering asymmetries are related to those of the neutron through effective nucleon polarization in ^{3}He for DIS

$$A^{^3He} = \frac{A^n P^n \sigma^n + 2A^p P^p \sigma^p}{\sigma^n + 2\sigma^p} \ , \tag{8}$$

or inversely

$$A^n = \frac{1}{f^n P^n} \left(A^{^3He} - (1 - f^p) A^p P^p \right) \ , \tag{9}$$

where the proton dilution factor $f^p \equiv \sigma^n/(\sigma^n + 2\sigma^p)$, which is only related to the ratio of proton to neutron cross sections σ^p/σ^n. The effective polarizations, based on nuclear physics

calculations are

$$P^n = +0.86^{+0.036}_{-0.02} \tag{10}$$

$$P^p = -0.028^{+0.009}_{-0.004} \tag{11}$$

$$. \tag{12}$$

The uncertainty due to the small proton effective polarization of -2.8% is estimated at: (uncertainty in proton polarization) $\times$ (maximum asymmetry ratio) $\times$ (maximum cross section ratio $2\sigma_p/\sigma_n$) $\sim$ 4%.

D. Radiative Corrections

The internal radiation correction effects are calculated in [107] and found to be small (about 1%). The plan is to include them in the MC, which will account also for external radiation. The contamination from exclusive channels is estimated from Monte Carlo to be less than 3%.

TABLE I: Budget for systematic uncertainties.

Source	Type	A_{LL}
Raw asymmetries	absolute	negligible
Random coincidences	relative	1%
Polarimetry	relative	6%
Nuclear corrections	relative	4%
Radiative corrections	relative	1%
Total	absolute relative	negligible 8%

VI. COLLABORATION RESPONSIBILITIES

If approved and funded, the four co-spokespersons are committed to working to realize this program of measurements in a timely fashion with the highest priority. Specifically:

A. Target Development

If given scientific approval, and funding for the target becomes available, James Maxwell will initiate the target development project at Jefferson Lab, with the support of the Jefferson Lab Target Group. In the last two decades this group has designed, built and operated the Q-weak cryotarget, FROST frozen spin target, g_2^p/G_E^p polarized solid target, PRad cryogenic windowless gas target, MARATHON tritium target, and GlueX cryotarget, among others. Richard Milner, with technical support from MIT-Bates, and Hadronic Physics Group student and post-doc participation, will collaborate on the target development. His group has played a leading role in design, construction and operation of polarized ^{3}He gas targets based on MEOP at MIT-Bates, the IUCF Cooler and the HERMES experiment at DESY.

B. Simulation and Analysis

Dien Thi Nguen and Harut Avakian will coordinate the efforts on studies of the 3D partonic distributions, from single and double spin asymmetries measured in production of all accessible final state hadrons and photons. Or Hen and his MIT-LNS Hadronic Physics Group will collaborate on simulation and analysis.

There is an active CLAS12 working group focused on physics opportunities with a polarized ^{3}He target, coordinated by Richard Milner. This initial proposal sprung from discussion within this working group. If the target development proceeds, it is anticipated that further proposals will be forthcoming. Finally, we welcome all interested physicists who are interested in contributing to make the proposed program a reality.

VII. SUMMARY

We propose a measurement of the neutron spin and azimuthal asymmetries A_{UL} and A_{LL} in semi-inclusive electroproduction of charged pions for 30 PAC days, using the 10.6 GeV CEBAF polarized electron beam and a new polarized ^{3}He target located in the central solenoid of the CLAS12 spectrometer. High precision 4-D (x, z, p_T, Q^2) data on the neutron will constrain present theoretical ideas of the nucleon spin structure described by QCD. The A_{LL} data will improve the the precision of the determination of the d quark helicity distribution in the nucleon.

The statistical projections assume 30 days of continuous 100% data taking at an incident energy of 10.6 GeV and 2 μA of 80% polarized electron beam providing a luminosity of 4.5×10^{34} ^{3}He/cm^2/s. Assuming 50% efficiency, we request 60 days of beamtime.

The requested beam intensity is significantly higher than the typical operating intensity in Hall B so the hall radiation protection system and the beam dump will have to modified to allow operation of the increased intensity.

VIII. OTHER SCIENTIFIC OPPORTUNITIES

The focus of this initial proposal is on the measurement of inclusive DIS and SIDIS on a longitudinally polarized neutron. However, a polarized ^{3}He target in CLAS12 presents many further scientific opportunities to study the quark and gluon structure of both the neutron as well as a few-body nucleus. These opportunities would capitalize on existing capabilities and developments, be complementary to planned experiments using polarized proton and deuteron targets, and open up new scientific vistas that lead naturally to the EIC. However, they stand distinct from what can be accomplished at EIC and are uniquely accessible in the Jefferson Lab 12 GeV era, i.e. in the coming decade and beyond. This collaboration has started to work to systematically consider these opportunities.

- *Higher Twist SSAs in SIDIS*

  Worldwide studies of different polarized structure functions indicate that the higher twist contributions including $F_{LU}^{\sin\phi}$, $F_{UL}^{\sin\phi}$, $F_{LL}^{\cos\phi}$, can be very significant. They provide access to elusive quark-gluon correlations [97] and will be also studied with high precision in proposed measurement. Some were already studied with CLAS, and extended range in Q^2 will help to define their higher twist nature. One example are significant azimuthal modulations of double spin asymmetries $A_{LL}^{\cos\phi}$ for all hadrons, predicted for the large x region covered by proposed measurement [43, 108].

- *Deeply Virtual Compton Scattering (DVCS)*

  It is widely recognized that the cleanest process to access generalized Parton Distributions (GPD)is DVCS. Nuclear GPDs cannot be trivially inferred from those of nuclear parton distributions functions, as determined in DIS. A calculation of extracting neutron generalized parton distributions from ^{3}He data finds [109] that coherent DVCS at low Δ^2 is strongly dominated by the neutron contribution. In this work, a procedure has been developed to take into account the nuclear effects included in the impulse approximation analysis and to safely disentangle the neutron contribution from them.

- *Deeply Virtual Meson Production (DVMP)*

  GPDs can also be accessed via exclusive meson electroproduction. Both pseudoscalar, e.g. π^0 and η, and vector, e.g. ϕ, meson production are of interest. The pseudoscalar channel has potential access to quark transversity GPDs, which can provide transverse

images of transversely polarized quarks in the valence quark region [110, 111]. The vector mesons have the potential to provide information on the transverse spatial distribution of gluons [112].

- *Transverse Target Polarization*

  Extension of the SIDIS measurements proposed here to a transversely polarized ^{3}He target will provide access to Transverse Momentum Distributions (TMDs) of the neutron in the valence quark region. High luminosity with a large kinematic coverage will allow access to three-dimensional, spin-correlated distributions of quarks and gluons of the nucleon in momentum space. The combination of single-spin and double-spin asymmetries for both longitudinally and transversely polarized ^{3}He targets with charged pion and kaon detection over a large kinematic range will give unprecedented access to the 3D structure of the neutron.

- *Tagged DIS*

  Development of the technical ability to detect the spectator nucleon in coincidence with the violent DIS event on the accompanying nucleon in a few-body nucleus has been a major focus of effort at Jefferson Lab, e.g. TDIS in Hall A [113] and BONuS [114] and ALERT [115] in Hall B. The possibility of low-energy proton and deuteron detection from a polarized ^{3}He target located in the central solenoid in CLAS12, raises the exciting possibilities to measure the DIS spin-dependent structure functions of the proton and deuteron in the bound ^{3}He nucleus [116]. Precise comparison with the unbound proton and deuteron observables can provide a stringent test of possible medium modifications of the quark polarizations. Co-existence of a recoil detector and polarized ^{3}He target within the CLAS12 central solenoid will be technically challenging.

- *Quasielastic Scattering*

  At low Q^2, quasielastic spin-dependent electron scattering from polarized ^{3}He explores the spin-dependent spectral function $S_{\sigma_A}(E, \mathbf{p}, t)$, defined as the probability density of finding a nucleon N of isospin t with energy E, momentum $\mathbf{p}$ and spin σ_N parallel (or antiparallel) to the $\overrightarrow{^3\text{He}}$ nucleus. It is calculated [117] using Faddeev techniques and has been measured experimentally, in limited kinematics [118]. It is an essential ingredient to convolution models that calculate spin-dependent DIS or SIDIS from polarized ^{3}He. The final-state in quasielastic electron scattering from ^{3}He can be both

two-body and three-body and the asymmetries are very different depending upon the final-state. It is anticipated that the optimal running configuration will use a lower beam energy and demand high performance in energy resolution from the detector.

Appendix A: Summary of Rates

Table II summarizes the total numbers of events projected in inclusive DIS and in the different SIDIS channels for different cuts for the 30 day run. By comparison, the previous experiments from polarized ^{3}He at SLAC, E142 and E154, accumulated $100 - 300$ M DIS inclusive events.

TABLE II: Projected total number of events for the 30 day run in this proposal.

Reaction	No. of events (Millions)	Cuts
DIS inclusive	4,000	$Q^2 > 1$, $W^2 > 4$
(e,e'π^+)	2,200	$Q^2 > 1$, $W^2 > 4$
(e,e'π^-)	1,200	$Q^2 > 1$, $W^2 > 4$
(e,e'K^+)	253	$Q^2 > 1$, $W^2 > 4$
(e,e'K^-)	60	$Q^2 > 1$, $W^2 > 4$
(e,e'π^+)	590	$Q^2 > 1$, $W^2 > 4$, z >0.3
(e,e'π^-)	210	$Q^2 > 1$, $W^2 > 4$, z >0.3
(e,e'K^+)	142	$Q^2 > 1$, $W^2 > 4$, Z >0.3
(e,e'K^-)	25	$Q^2 > 1$, $W^2 > 4$, z >0.3

Appendix B: 2D Asymmetry Absolute Uncertainty Estimation for Charged Pion SIDIS

General event selection cuts were applied: $Q^2 > 1$, $W^2 > 4$, $M_{miss} > 1.4$ and $y < 0.85$, the cut on $z > 0.3$ was also applied to select leading hadrons. The statistical uncertainty in the asymmetry is calculated as a function of (Q^2 vs x), (x vs z), (x vs p_T) and (z vs p_T).

Fig. 32 shows the accessible Q^2 vs. x region for $z > 0.3$.

Fig. 33 shows the accessible x vs. z region.

Fig. 34 shows the accessible region for x vs p_T for $z > 0.3$.

Fig. 35 shows the accessible region z vs p_T for the valence quark region $0.2 < x < 0.4$,

Fig. 36 shows the accessible region z vs p_T for the sea quark region $0.05 < x < 0.1$,

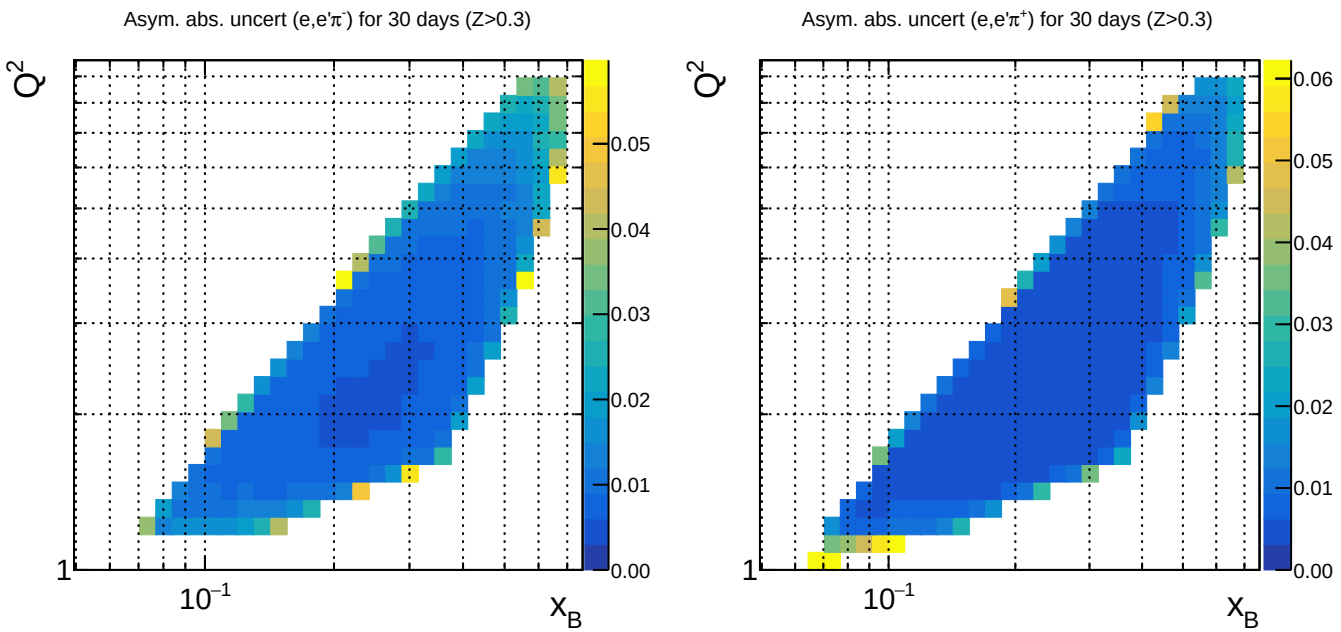

FIG. 32: Q^2 vs x for $z > 0.3$.

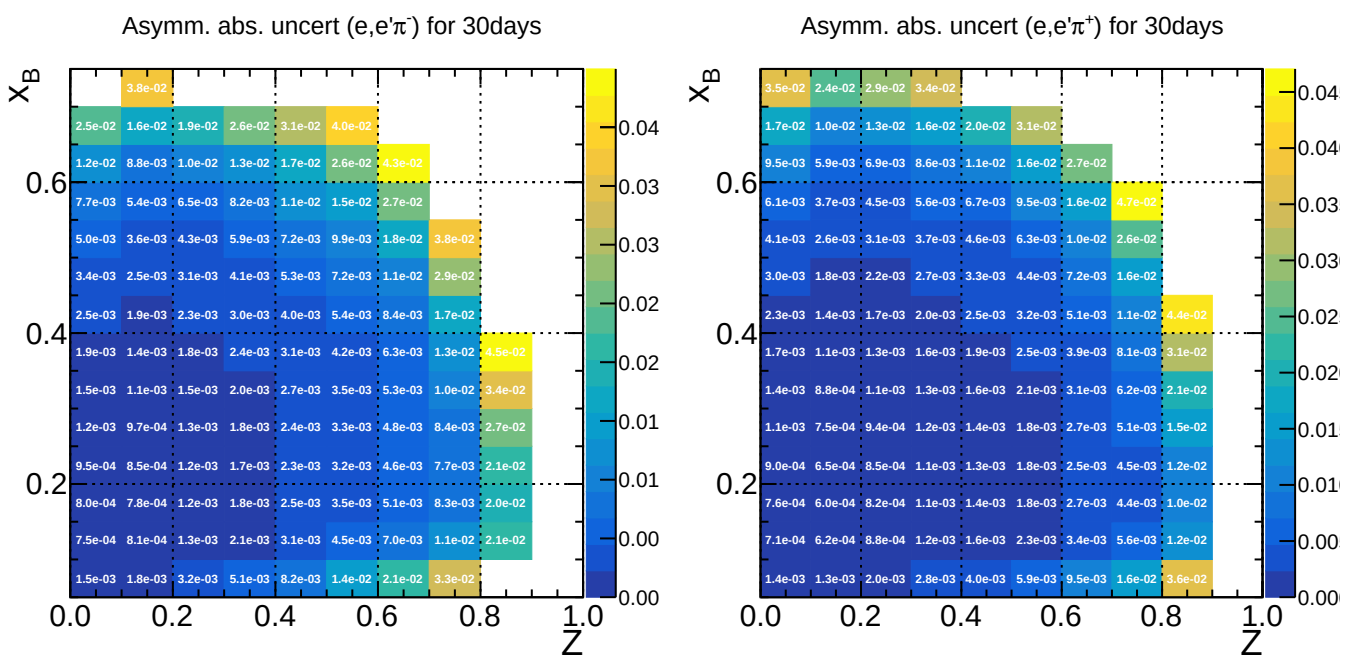

FIG. 33: x vs z.

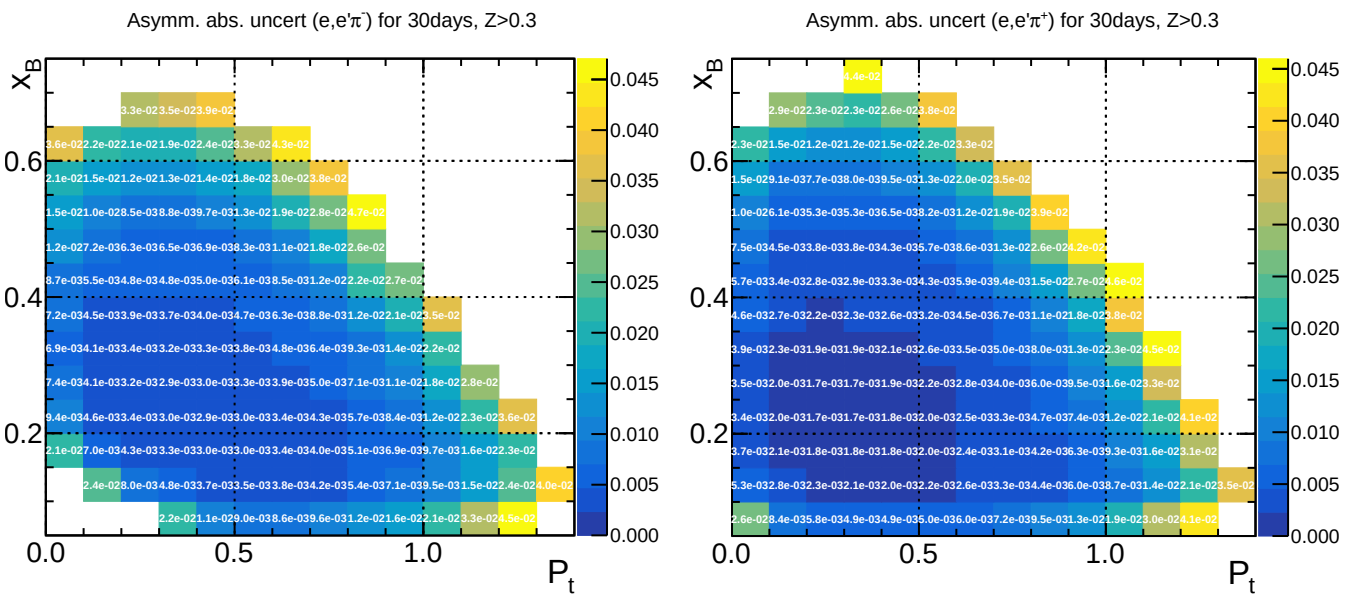

FIG. 34: x vs p_T for $z > 0.3$.

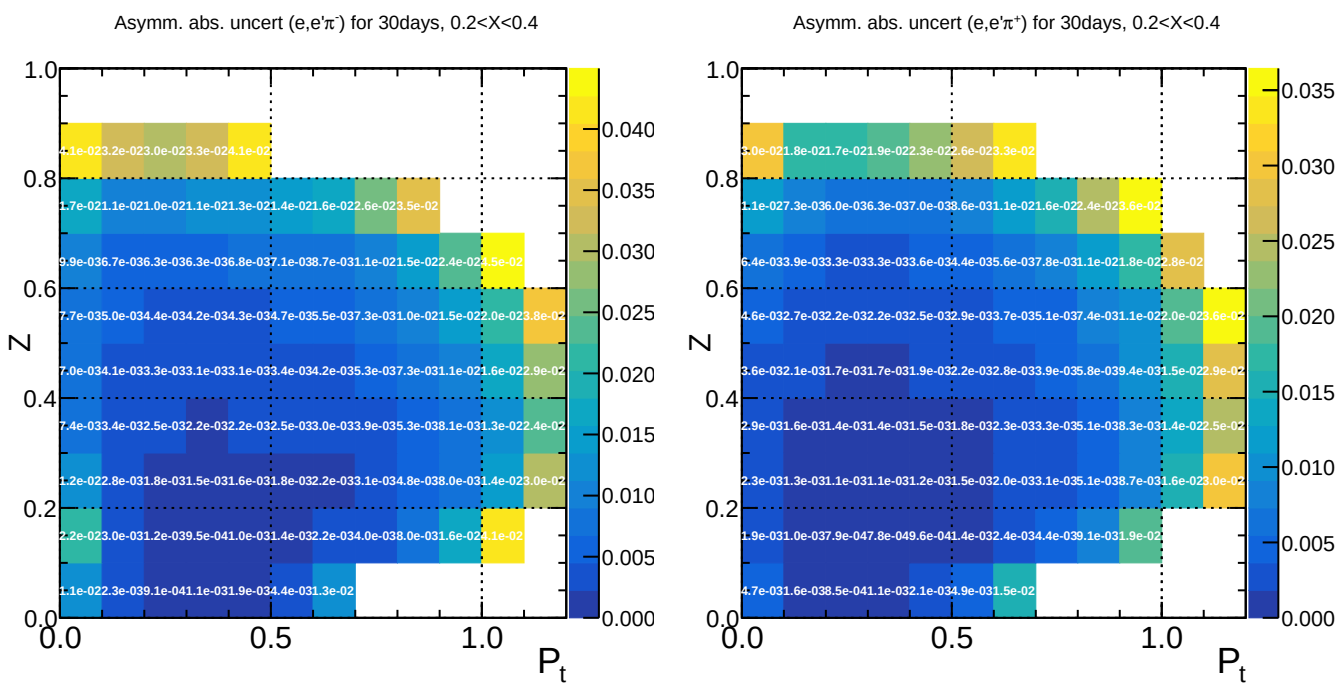

FIG. 35: z vs p_T for the valence quark region $0.2 < x < 0.4$.

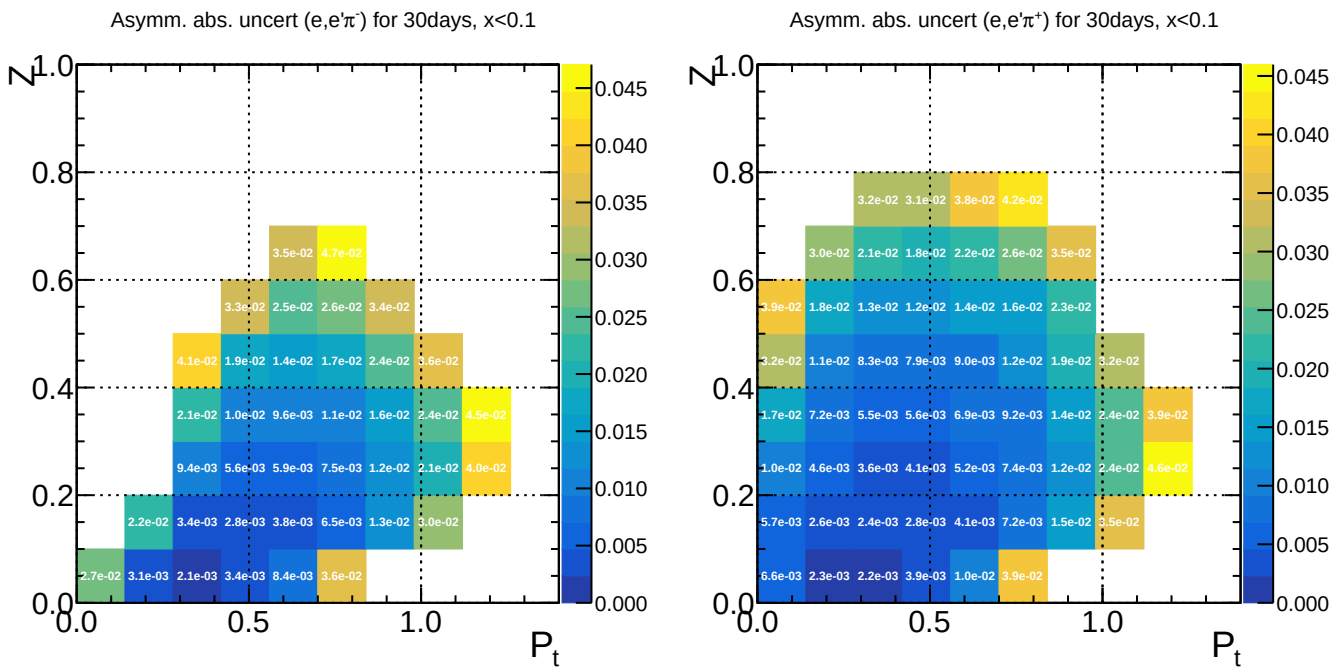

FIG. 36: z vs P_T for sea quark region $0.05 < x < 0.1$.

Appendix C: 2D Asymmetry Absolute Uncertainty Estimation for Charged Kaon SIDIS

The same event selection as used for pions was used for kaons to estimate the asymmetry absolute uncertainty in 2D plots.

Fig. 37 shows the accessible region Q^2 vs x for $z > 0.3$.

Fig. 38 shows the accessible region x vs z,

Fig. 39 shows the accessible region x vs p_T for $z > 0.3$,

Fig. 40 shows the accessible region z vs p_T.

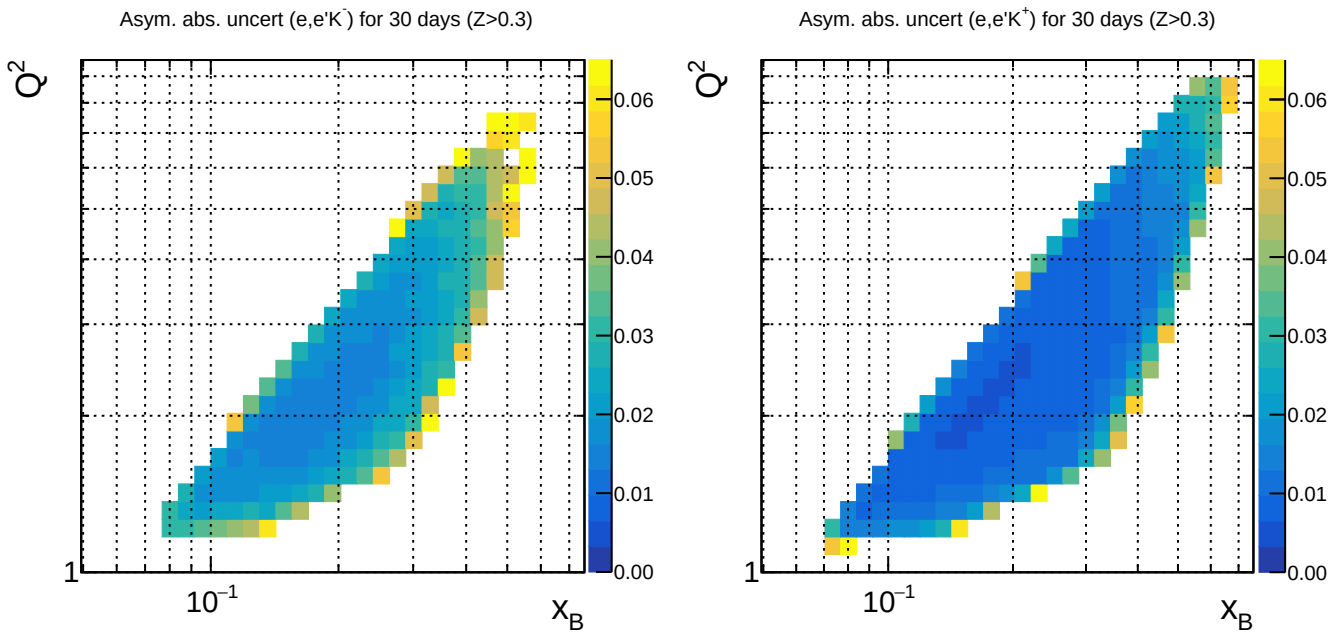

FIG. 37: Q^2 vs x for $z > 0.3$.

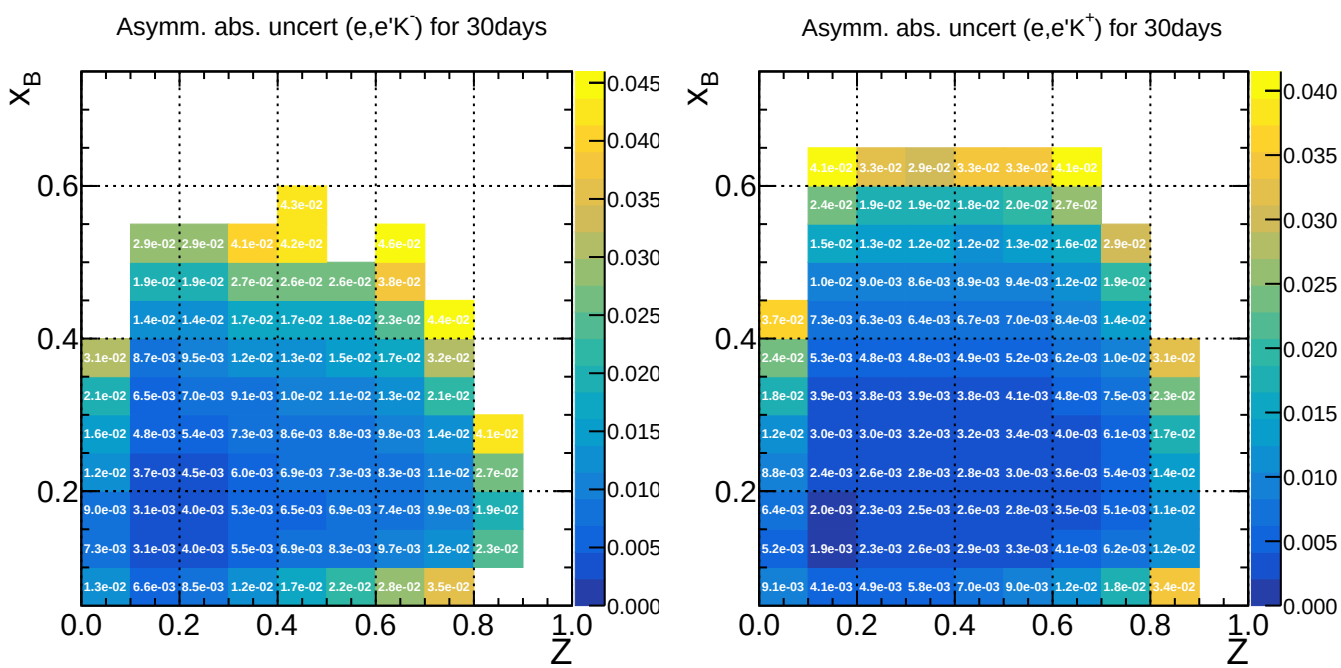

FIG. 38: x vs z.

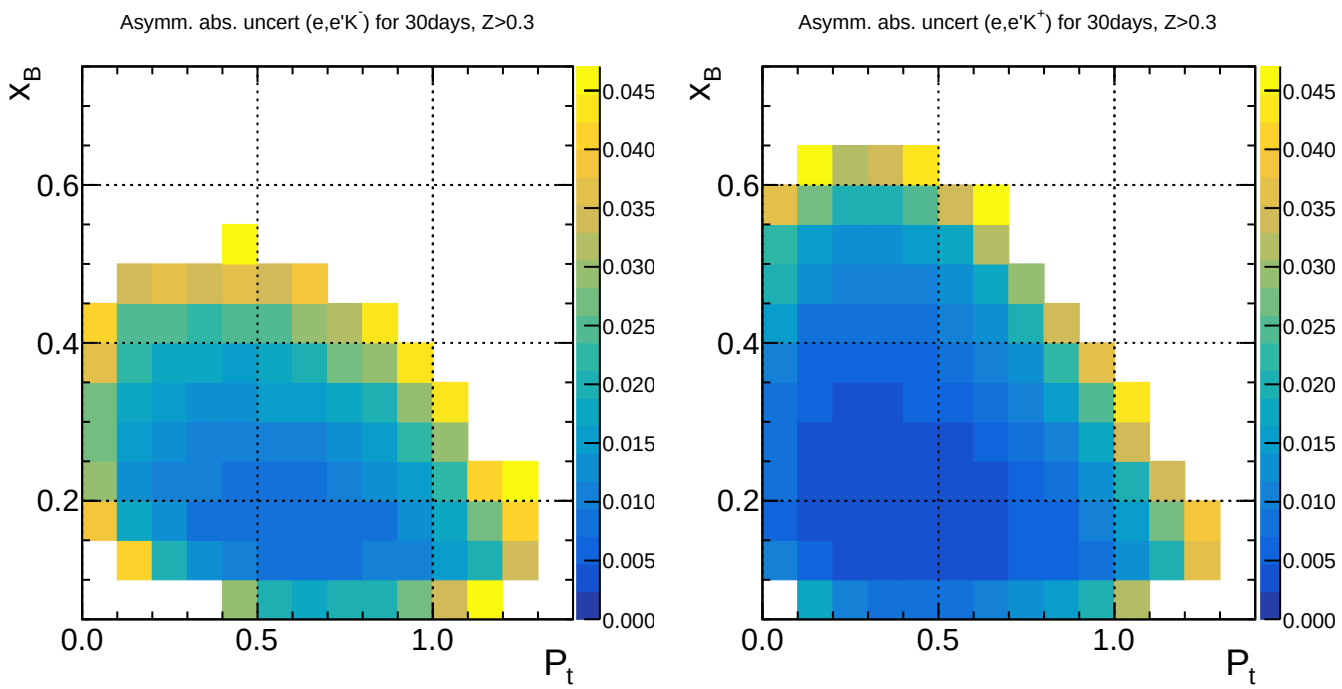

FIG. 39: x vs p_T for $z > 0.3$.

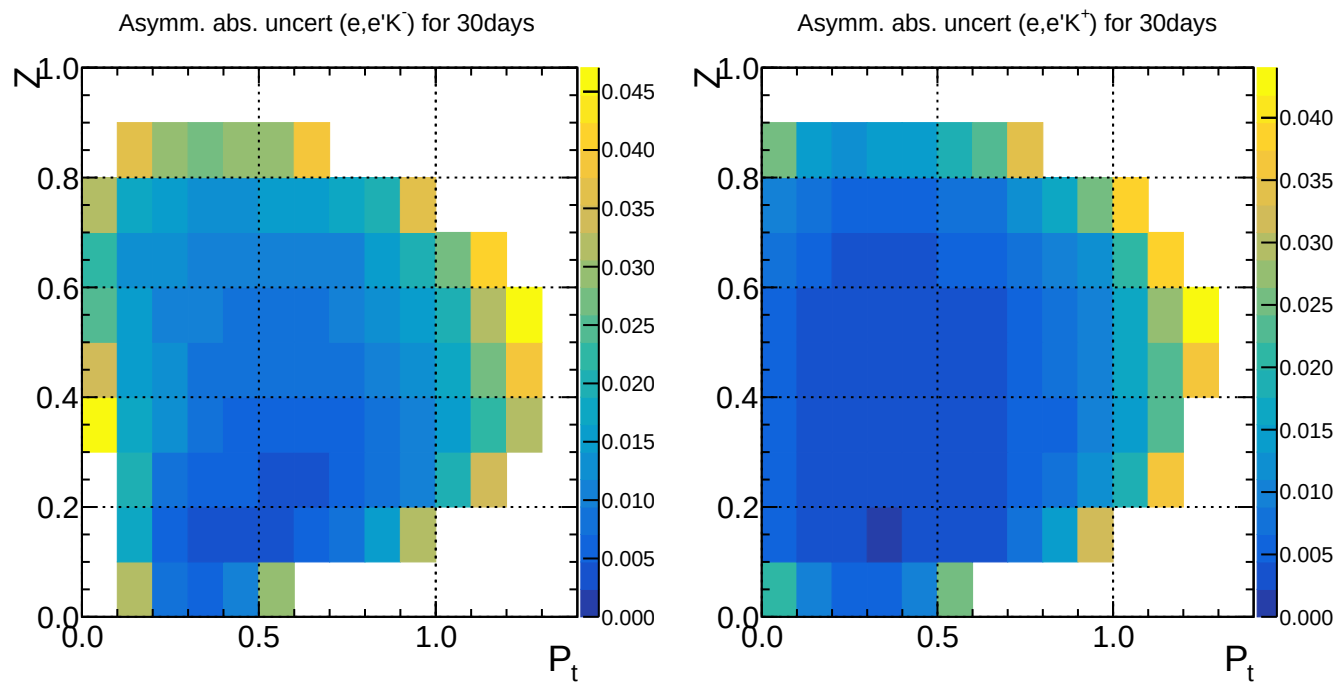

FIG. 40: z vs p_T.

Appendix D: Logarithmic Binning

Table III describes the 28×28 logarithmic binning in x and Q^2 used in this proposal.

TABLE III: Binning in x and Q^2 used in this proposal.

Q^2_{min}	Q^2_{max}		x_{min}	x_{max}
1.000	1.0081		0.5900	0.0644
1.081	1.169		0.0644	0.0704
1.169	1.265		0.0704	0.0768
1.265	1.367		0.0768	0.0839
1.367	1.479		0.0839	0.0917
1.479	1.599		0.0917	0.1001
1.599	1.729		0.1001	0.1093
1.729	1.870		0.1093	0.1194
1.870	2.022		0.1194	0.1304
2.022	2.187		0.1304	0.1424
2.187	2.365		0.1424	0.1555
2.365	2.557		0.1555	0.1699
2.557	2.765		0.1699	0.1855
2.765	2.990		0.1855	0.2026
2.990	3.234		0.2026	0.2213
3.234	3.497		0.2213	0.2417
3.497	3.781		0.2417	0.2639
3.781	4.089		0.2639	0.2882
4.089	4.422		0.2882	0.3148
4.422	4.782		0.3148	0.3438
4.782	5.171		0.3438	0.3755
5.171	5.592		0.3755	0.4101
5.592	6.047		0.4101	0.4479
6.047	6.539		0.4479	0.4891
6.539	7.071		0.4891	0.5342
7.071	7.646		0.5342	0.5834
7.646	8.269		0.5834	0.6372
8.269	8.942		0.6372	0.6959

Appendix E: Comparison to Completed and Planned Experiments

TABLE IV: Summary of completed (upper section) and planned (lower section) high-energy, spin-dependent electron scattering experiments from polarized ^{3}He over the last three decades.

Experiment	**Year**	**E_0** GeV	**Lumi** ^{3}He cm^{-2} s^{-1}	**Solid angle** msr	**DIS**	**SIDIS**
E-142 [119]	1992	19.4 to 25.5	5.2×10^{34}	0.7	300 M events $0.03 < x < 0.6$ $< Q^2 > = 2$	None
E-154 [120]	1995	48.3	5.2×10^{34}	0.7	100 M events $0.014 < x < 0.7$ $< Q^2 > = 5$	None
HERMES [121]	1995	27.5	4×10^{31}	500	3 M events $0.023 < x < 0.6$ $< Q^2 > = 2.3$	Only h^+, h^-
E99-117 Hall A [122]	2001	5.73	5×10^{35}	7 HRS	$x = 0.33, 0.47, 0.60$ $Q^2 = 2.71, 3.52, 4.83$	None
E06-010/011 Hall A [123]	2009	5.9	5×10^{35} Trans. pol.	65 BigBite	$0.16 < x < 0.35$ $1.4 < Q^2 < 2.7$	π^+, π^- SSA
E06-014 Hall A [124]	2009	4.7,5.9	5×10^{35}	65 BigBite	$0.277 < x < 0.548$ $< Q^2 > = 3.078$	None
E12-06-110 Hall C[125]	2020	10.6	1×10^{36}	8 (HMS) 3.8 (SHMS)	$0.3 < x < 0.77$ $3 < Q^2 < 10$	None
E12-06-112 Hall A [36]		8.8, 6.6	2×10^{36}	HRS BigBite	$0.2 < x < 0.71$ $3 < Q^2 < 8$	None
SoLID E12-11-007[35, 126]		8.8, 11	2×10^{36}	0.5×10^3 SOLID	$0.05 < x < 0.65$ $0.3 < z < 0.7$ $1 < Q^2 < 8$	π^+, π^-
CLAS12 (this proposal)		10.6	4.5×10^{34}	10^4	4000 M events $0.05 < x < 0.7$ $1 < Q^2 < 9$ $W^2 > 4$	π^+, π^-, K^+, K^- Di-hadrons $0.2 < z < 0.9$ $0.2 < p_T < 1.3$

Appendix F: Model Calculations of Spin Asymmetries

The structure functions describing inclusive hadron production in SIDIS, $ep \to e'hX$, off a nucleon N (p,n), can be written as:

$$F_{UU}^N = \sum_q e_q^2 \int d^2\boldsymbol{k}_\perp \, f_1^{q/N} \, D_{h/q} = \mathcal{C}[f_1 \, D_1] \tag{F1}$$

$$F_{LL}^N = \sum_q e_q^2 \int d^2\boldsymbol{k}_\perp \, g_{1L}^{q/N} \, D_{h/q} = \mathcal{C}[g_{1L}^{q/p} \, D_1]. \tag{F2}$$

If we take a Gaussian ansatz [89] for TMD quark distributions in a nucleon, the integrations in the leading twist contributions F_{UU}^N and F_{LL}^N can be carried out analytically. We assume the x and $k_\perp$ dependences to be factorized and we assign the $k_\perp$ dependence a Gaussian distribution with one free parameter to fix the Gaussian width for a given flavor q. For the unpolarized and helicity distribution functions and for the fragmentation function we use,

$$f_1^{q/N}(x, k_\perp) = f_1^{q/N}(x) \, \frac{e^{-k_\perp^2/\langle k_\perp^2 \rangle^q}}{\pi \langle k_\perp^2 \rangle^q}, \tag{F3}$$

$$g_{1L}^{q/N}(x, k_\perp) = g_{1L}^{q/N}(x) \, \frac{e^{-k_\perp^2/\langle k_\perp^2 \rangle_L^q}}{\pi \langle k_\perp^2 \rangle_L^q}, \tag{F4}$$

$$D_{h/q}(z, p_\perp) = D_{h/q}(z) \, \frac{e^{-p_\perp^2/\langle p_\perp^2 \rangle}}{\pi \langle p_\perp^2 \rangle}, \tag{F5}$$

where $f_1^{q/N}(x)$, $g_{1L}^{q/N}(x)$ and $D_{h/q}(z)$ have been taken from the available fits of the world data, and for calulations we assume $u/p = d/n$. The widths of the Gaussians for partonic distributions were normally assumed [43, 127] different only different helicities, with no flavor dependence. The widths of quark distributions in general will depend also on the flavor and on the relative orientation of the polarizations of quark and the parent nucleon [46]. The numbers extracted from Lattice calculations of those widths were used to study the sensitivity of double spin asymmetry for pions on flavor and spin dependence of underlying k_T-distributions of quarks.

After the $\boldsymbol{k}_\perp$ integrations analytically in Eqs. (F1-F2), we can re-express all structure functions in terms of the Gaussian parameters by using:

$$\int d^2\boldsymbol{k}_\perp \, d^2\boldsymbol{p}_\perp \, \delta^{(2)}(\boldsymbol{p}_{hT} - z_h \boldsymbol{k}_\perp - \boldsymbol{p}_\perp) \, \frac{e^{-k_\perp^2/\langle k_\perp^2 \rangle}}{\pi \langle k_\perp^2 \rangle} \, \frac{e^{-p_\perp^2/\langle p_\perp^2 \rangle}}{\pi \langle p_\perp^2 \rangle} = \frac{e^{-P_T^2/\langle P_T^2 \rangle}}{\pi \langle P_T^2 \rangle}.$$

[1] D. R. Phillips, Ann. Rev. Nucl. Part. Sci. **66**, 421 (2016).

[2] T. R. Gentile, P. J. Nacher, B. Saam, and T. G. Walker, Rev. Mod. Phys. **89**, 045004 (2017).

[3] S. Kuhn, D. Crabb, A. Deur, T. Forest, K. Griffioen, M. Holtrop, and Y. Prok, *The Longitudinal Spin Structure of the Nucleon*, Proposal E12-06-109.

[4] S. Niccolai, A. Biselli, C. Keith, S. Pisano, and D. Sokhan, *Deeply virtual Compton scattering on the neutron with a longitudinally polarized deuteron target*, Proposal E12-06-109A.

[5] B. Wojtsekhowski, G. Cates, E. Cisbani, G. Franklin, and A. Puckett, *Measurement of the Semi-Inclusive π and K electro-production in DIS regime from transversely polarized ^{3}He target with the SBS & BB spectrometers in Hall A*, Proposal E12-09-18.

[6] H. Gao, J. Chen, X. Jiang, J. Peng, and X. Qian, *An update to PR12-09-014: Target Single Spin Asymmetry in Semi-Inclusive Deep-Inelastic Electro-Pion Production on a Transversely Polarized ^{3}He Target at 8.8 and 11 GeV*, Proposal E12-10-006.

[7] J. Chen, Y. Qiang, and Y. Yan, *Asymmetries in Semi-Inclusive Deep-Inelastic Electro-Production of Charged Pions on a Longitudinally Polarized ^{3}He Target at 8.8 and 11 GeV*, Proposal E12-11-007.

[8] J. Maxwell and R. Milner, *Conceptual Design of a Polarized ^{3}He Target for the CLAS12 Spectrometer*, arXiv: 1911.06650 (2019).

[9] W. Chen *et al.*, *Polarized ^{3}He cell development and application at NIST*, Journal of Physics: Conference Series **294**, 012003 (2011).

[10] C. E. Jones, *A Measurement of the Spin-Dependent Asymmetry in Quasielastic Scattering of Polarized Electrons from Polarized ^{3}He*, Ph.D. thesis, Caltech (1992).

[11] E. Courtade *et al.*, Hyperfine Interactions **127**, 451 (2000).

[12] A. Nikiel-Osuchowska *et al.*, The European Physical Journal D **67**, 200 (2013).

[13] J. Maxwell, C. Epstein, R. Milner, J. Alessi, E. Beebe, A. Pikin, J. Ritter, and A. Zelenski, *Proceedings, 21st International Symposium on Spin Physics (SPIN 2014): Beijing, China, October 20-24, 2014*, Int. J. Mod. Phys. Conf. Ser. **40**, 1660102 (2016).

[14] K. Suchanek *et al.*, The European Physical Journal Special Topics **144**, 67 (2007).

[15] J. Maxwell *et al.*, Nucl. Instr. and Meth. A **959**, 161892 (2020).

[16] V. Lefevre-Seguin and J. Brossel, Journal of Low Temperature Physics **72**, 165.

[17] R. Milner, R. McKeown, and C. Woodward, Nucl. Instr. and Meth. A **274**, 56 (1989).

[18] K. Bonin, T. Walker, and W. Happer, Physical Review A **37**, 3270 (1988).

[19] E. Pasyuk, personal communication.

[20] M. Statera *et al.*, Nucl. Instr. and Meth. A **882**, 17 (2018).

[21] M. Beckmann, HERMES collaboration (1999).

[22] A. Kotzinian, Nucl. Phys. **B441**, 234 (1995), arXiv:hep-ph/9412283 [hep-ph].

[23] P. Mulders and R. Tangerman, Nucl. Phys. B **461**, 197 (1996), [Erratum: Nucl.Phys.B 484, 538–540 (1997)], arXiv:hep-ph/9510301.

[24] A. Bacchetta *et al.*, JHEP **02**, 093 (2007), arXiv:hep-ph/0611265.

[25] M. Alberg and G. A. Miller, arXiv:1712.05814 (2017), arXiv:1712.05814 [nucl-th].

[26] P. Amaudruz *et al.* (New Muon), Phys. Rev. Lett. **66**, 2712 (1991).

[27] G. T. Garvey and J.-C. Peng, Prog. Part. Nucl. Phys. **47**, 203 (2001), arXiv:nucl-ex/0109010 [nucl-ex].

[28] K. Nagai, *Proceedings, 14th International Conference on Meson-Nucleon Physics and the Structure of the Nucleon (MENU 2016): Kyoto, Japan, July 25-30, 2016*, JPS Conf. Proc. **13**, 020051 (2017).

[29] J. Dudek *et al.*, Eur. Phys. J. **A48**, 187 (2012), arXiv:1208.1244 [hep-ex].

[30] R. Ent *et al.*, JLab Experiment E12-06-104 (2006).

[31] R. Ent *et al.*, JLab Experiment E12-09-017 (2009).

[32] R. Ent *et al.*, JLab Experiment E12-13-007 (2013).

[33] G. Cates, E. Cisbani, G. Franklin, A. Puckett, and W. B., JLab Experiment E12-09-018 (2009).

[34] H. Gao, Q. X., and P. J.-C., JLab Experiment E12-10-006 (2008).

[35] J.-P. Chen, J. Huang, Y. Qiang, and Y. Wenbiao, JLab Experiment E12-11-007 (2008).

[36] T. Averett, G. Cates, N. Liyanage, G. Rosner, B. Wojtsekhowski, and Z. X., *Measurement of neutron spin asymmetry A_1^n in the valence quark region using 8.8 GeV and 6.6 GeV beam energy and Bigbite spectrometer in Hall A*, Proposal E12-06-112.

[37] H. Avakian *et al.*, JLab Experiment E12-07-107 (2007).

[38] H. Avakian *et al.*, JLab Experiment E12-09-008 (2009).

[39] H. Avakian *et al.*, JLab Experiment E12-09-009 (2009).

[40] A. Signori, A. Bacchetta, M. Radici, and G. Schnell, JHEP **1311**, 194 (2013),

arXiv:1309.3507 [hep-ph].

[41] B. Pasquini, S. Cazzaniga, and S. Boffi, Phys. Rev. **D78**, 034025 (2008), arXiv:hep-ph/0806.2298 [hep-ph].

[42] Z. Lu and B.-Q. Ma, Nucl. Phys. **A741**, 200 (2004), arXiv:hep-ph/0406171.

[43] M. Anselmino, A. Efremov, A. Kotzinian, and B. Parsamyan, Phys. Rev. D **74**, 074015 (2006), arXiv:hep-ph/0608048.

[44] C. Bourrely, F. Buccella, and J. Soffer, Phys.Rev. **D83**, 074008 (2011), arXiv:1008.5322 [hep-ph].

[45] P. Hagler, B. U. Musch, J. W. Negele, and A. Schafer, Europhys. Lett. **88**, 61001 (2009), arXiv:hep-lat/0908.1283 [hep-lat].

[46] B. U. Musch, P. Hagler, J. W. Negele, and A. Schafer, Phys.Rev. **D83**, 094507 (2011), arXiv:1011.1213 [hep-lat].

[47] M. Wakamatsu, Phys. Rev. **D79**, 094028 (2009), arXiv:0903.1886 [hep-ph].

[48] P. Schweitzer, M. Strikman, and C. Weiss, JHEP **1301**, 163 (2013), arXiv:1210.1267 [hep-ph].

[49] M. Anselmino, M. Boglione, J. Gonzalez H., S. Melis, and A. Prokudin, JHEP **1404**, 005 (2014), arXiv:1312.6261 [hep-ph].

[50] A. Bacchetta, F. Delcarro, C. Pisano, M. Radici, and A. Signori, JHEP **06**, 081 (2017), arXiv:1703.10157 [hep-ph].

[51] A. Airapetian *et al.* (HERMES), Phys. Rev. Lett. **84**, 4047 (2000), hep-ex/9910062.

[52] A. M. Kotzinian and P. J. Mulders, Phys. Rev. **D54**, 1229 (1996), hep-ph/9511420.

[53] R. D. Tangerman and P. J. Mulders, Phys. Rev. **D51**, 3357 (1995), hep-ph/9403227.

[54] S. J. Brodsky and F. Yuan, Phys. Rev. **D74**, 094018 (2006), hep-ph/0610236.

[55] P. V. Pobylitsa, hep-ph/0301236 (2003), arXiv:hep-ph/0301236 [hep-ph].

[56] A. V. Efremov, K. Goeke, and P. Schweitzer, Phys. Rev. **D67**, 114014 (2003), hep-ph/0208124.

[57] H. Avakian *et al.* (CLAS Collaboration), Phys. Rev. Lett. **105**, 262002 (2010), arXiv:hep-ex/1003.4549 [hep-ex].

[58] B. Parsamyan, *Proceedings, 25th International Workshop on Deep-Inelastic Scattering and Related Topics (DIS 2017): Birmingham, UK, April 3-7, 2017*, arXiv:1801.01488 **DIS2017**, 259 (2018), arXiv:1801.01488 [hep-ex].

[59] B. Parsamyan, PoS **QCDEV2017**, 042 (2018).

[60] S. Jawalkar *et al.*, Phys. Lett. **B782**, 662 (2018), arXiv:1709.10054 [nucl-ex].

[61] H. Avakian *et al.*, Phys. Rev. **D77**, 014023 (2008), arXiv:hep-ph/0709.3253 [hep-ph].

[62] X. Ji and F. Yuan, Phys. Lett. **B543**, 66 (2002), hep-ph/0206057.

[63] S. J. Brodsky, D. S. Hwang, and I. Schmidt, Phys. Lett. **B530**, 99 (2002), hep-ph/0201296.

[64] S. J. Brodsky, D. S. Hwang, and I. Schmidt, Nucl. Phys. **B642**, 344 (2002), hep-ph/0206259.

[65] A. Bacchetta, A. Schäafer, and J.-J. Yang, Phys. Lett. **B578**, 109 (2004), hep-ph/0309246.

[66] L. P. Gamberg, G. R. Goldstein, and K. A. Oganessyan, Phys. Rev. **D67**, 071504 (2003), hep-ph/0301018.

[67] S. Meissner, A. Metz, and K. Goeke, Phys. Rev. **D76**, 034002 (2007), arXiv:hep-ph/0703176.

[68] L. P. Gamberg, G. R. Goldstein, and M. Schlegel, Phys. Rev. **D77**, 094016 (2008), arXiv:hep-ph/0708.0324 [hep-ph].

[69] A. Bacchetta, L. P. Gamberg, G. R. Goldstein, and A. Mukherjee, Phys. Lett. **B659**, 234 (2008), arXiv:hep-ph/0707.3372 [hep-ph].

[70] A. Bacchetta, F. Conti, and M. Radici, Phys.Rev. **D78**, 074010 (2008), arXiv:0807.0323 [hep-ph].

[71] P. Schweitzer, T. Teckentrup, and A. Metz, Phys. Rev. **D81**, 094019 (2010), arXiv:1003.2190 [hep-ph].

[72] H. Avakian, A. V. Efremov, P. Schweitzer, and F. Yuan, Phys. Rev. **D81**, 074035 (2010), arXiv:hep-ph/1001.5467 [hep-ph].

[73] S. Boffi, , *et al.*, Phys. Rev. **D79**, 094012 (2009), arXiv:hep-ph/0903.1271 [hep-ph].

[74] B. Pasquini and F. Yuan, Phys. Rev. **D81**, 114013 (2010), arXiv:1001.5398 [hep-ph].

[75] B. Pasquini and P. Schweitzer, Phys.Rev. **D83**, 114044 (2011), arXiv:1103.5977 [hep-ph].

[76] B. Pasquini and P. Schweitzer, Phys.Rev. **D90**, 014050 (2014), arXiv:1406.2056 [hep-ph].

[77] B. U. Musch, *Transverse momentum distributions inside the nucleon from lattice QCD*, Ph.D. thesis, Munich, Tech. U. (2009-05), arXiv:0907.2381 [hep-lat].

[78] A. Airapetian *et al.* (HERMES), (2018), arXiv:1810.07054 [hep-ex].

[79] L. Kaptari *et al.*, Phys. Rev. C **89**, 035206 (2014).

[80] A. Del Dotto *et al.*, Few Body Syst. **55** (2014).

[81] L. Mankiewicz, A. Schafer, and M. Veltri, Comput. Phys. Commun. **71**, 305 (1992).

[82] A. Accardi, V. Guzey, A. Prokudin, and C. Weiss, Eur. Phys. J. **A48**, 92 (2012),

arXiv:1110.1031 [nucl-th].

[83] K. Ackerstaff *et al.*, Phys. Lett. B **464**, 123 (1999).

[84] M. Gluck, E. Reya, M. Stratmann, and W. Vogelsang, Phys. Rev. D **63**, 094005 (2001), arXiv:hep-ph/0011215.

[85] D. de Florian, R. Sassot, and M. Stratmann, J. Phys. Conf. Ser. **110**, 022045 (2008), arXiv:hep-ph/0708.0769 [hep-ph].

[86] A. Airapetian *et al.*, Phys. Rev. D **99**, 112001 (2019).

[87] S. Bastami *et al.*, JHEP **6**, 007 (2019).

[88] A. Kotzinian, B. Parsamyan, and A. Prokudin, Phys. Rev. D **73**, 114017 (2006), arXiv:hep-ph/0603194.

[89] S. Bastami *et al.*, JHEP **06**, 007 (2019), arXiv:1807.10606 [hep-ph].

[90] M. Glück, E. Reya, and A. Vogt, Eur. Phys. J. C **5**, 461 (1998), arXiv:hep-ph/9806404.

[91] S. Kretzer, Phys. Rev. D **62**, 054001 (2000), arXiv:hep-ph/0003177.

[92] A. D. Martin, W. J. Stirling, R. S. Thorne, and G. Watt, Eur. Phys. J. **C63**, 189 (2009), arXiv:0901.0002 [hep-ph].

[93] D. de Florian, R. Sassot, and M. Stratmann, Phys.Rev. **D75**, 114010 (2007), arXiv:hep-ph/0703242 [HEP-PH].

[94] M. Anselmino, M. Boglione, U. D'Alesio, S. Melis, F. Murgia, and A. Prokudin, Phys. Rev. D **87**, 094019 (2013), arXiv:1303.3822 [hep-ph].

[95] A. Metz and A. Vossen, Prog. Part. Nucl. Phys. **91**, 136 (2016), arXiv:1607.02521 [hep-ex].

[96] S. Pisano and M. Radici, Eur. Phys. J. A **52**, 155 (2016), arXiv:1511.03220 [hep-ph].

[97] H. Avakian, B. Parsamyan, and A. Prokudin, Riv. Nuovo Cimento **42**, 1 (2019).

[98] H. Avakian (CLAS), PoS **DIS2019**, 265 (2019).

[99] A. Courtoy, (2014), arXiv:1405.7659 [hep-ph].

[100] H. H. Matevosyan, A. Kotzinian, and A. W. Thomas, Phys. Rev. D **96**, 074010 (2017), arXiv:1707.04999 [hep-ph].

[101] A. Bacchetta and M. Radici, Phys. Rev. **D69**, 074026 (2004), arXiv:hep-ph/0311173.

[102] R. L. Jaffe and X.-D. Ji, Nucl. Phys. **B375**, 527 (1992).

[103] A. I. Signal, Nucl. Phys. **B497**, 415 (1997), arXiv:hep-ph/9610480.

[104] S. Sirtl, in *22nd International Symposium on Spin Physics* (2017) arXiv:1702.07317 [hep-ex].

[105] M. Burkardt, Phys. Rev. **D88**, 114502 (2013), arXiv:0810.3589 [hep-ph].

[106] M. Abdallah and M. Burkardt, Phys. Rev. D **94**, 094040 (2016), arXiv:1610.01166 [hep-ph].

[107] I. Akushevich, A. Ilyichev, and N. Shumeiko, arXiv:hep-ph/0106180 (2001).

[108] W. Mao, X. Wang, X. Du, Z. Lu, and B.-Q. Ma, Nucl. Phys. **A945**, 153 (2016).

[109] M. Rinaldi and S. Scopetta, Phys. Rev. C **87**, 035208 (2013).

[110] S. Goloskokov and P. Kroll, Eur. Phys. J. A **47**, 112 (2011).

[111] G. Goldstein *et al.*, Phys. Rev. D **91**, 114013 (2015).

[112] V. Goloskokov and P. Kroll, Eur. Phys. J. C **53**, 66201 (1996).

[113] C. Keppel *et al.*, *Measurement of Tagged Deep Inelastic Scattering (TDIS)*, Proposal PR12-15-006.

[114] H. Fenker *et al.*, Nucl. Instr. and Meth. A **592**, 273 (2008).

[115] K. Hafidi *et al.*, *Nuclear Exclusive and Semi-Inclusive Measurements with a New CLAS12 Low Energy Recoil Tracker*, Proposal PR12-16-011.

[116] R. Milner, *Spin-dependent DIS from Polarized* ^{3}*He at EIC*, Contribution to EIC Users Group Meeting Catholic University, Washington, DC, USA, July 2018 , arXiv: 1809.05626.

[117] R. Schulze and P. Sauer, Phys. Rev. C **48**, 38 (1993).

[118] M. Miller *et al.*, Phys. Rev. Lett. **74**, 502 (1995).

[119] P. Anthony *et al.*, Phys. Rev. D **54**, 114013 (2015).

[120] K. Abe *et al.*, Phys. Rev. Lett. **79**, 26 (1997).

[121] K. Ackerstaff *et al.*, Phys. Lett. B **404**, 383 (1997).

[122] X. Zheng *et al.*, Phys. Rev. Lett. **92**, 012004 (2004).

[123] X. Qian *et al.*, Phys. Rev. Lett. **107**, 072003 (2011).

[124] D. Parno *et al.*, Phys. Lett. B **744**, 309 (2015).

[125] X. Zheng, G. Cates, J. Chen, and Z. Meziani, *Measurement of neutron spin asymmetry* A_1^n *in the valence quark region using an 11 GeV beam and a Polarized* ^{3}*He target in Hall C*, Proposal E12-06-110.

[126] Private communication with J. P. Chen (2020)..

[127] M. Anselmino, M. Boglione, U. D'Alesio, S. Melis, F. Murgia, *et al.*, Phys.Rev. **D83**, 114019 (2011), arXiv:1101.1011 [hep-ph].